Ph. D. DISSERTATION

Experimental Investigation of the Nonlinear Electrokinetic Responses inside an Ion Depletion Zone

이온공핍영역 내부의 비선형성 전기동역학 반응 검증

BY

INHEE CHO

February 2018

Department of Electrical Engineering and Computer Science

Seoul National University

Experimental Investigation of the Nonlinear Electrokinetic Responses inside an Ion Depletion Zone

이온공핍영역 내부의 비선형성 전기동역학 반응 검증

지도교수 김 성 재

이 논문을 공학박사 학위논문으로 제출함

2018 년 2 월

서울대학교 대학원

전기컴퓨터공학부

조 인 희

조인희의 공학박사 학위논문을 인준함

2018년 2월

위 원 장 : 김 호 영 (인)

부위원장 : 김 성 재 (인)

위 원 : 곽 노 균 (인)

위 원 : 정 윤 찬 (인)

위 원 : 이 효 민 (인)

Experimental Investigation of the Nonlinear Electrokinetic Responses inside an Ion Depletion Zone

by

Inhee Cho

Advisor: Sung Jae Kim

A dissertation submitted in partial fulfillment of
the requirements for the degree of
Doctor of Philosophy
(Electrical Engineering and Computer Science)
in Seoul National University
February 2018

Doctoral Committee:

Professor Ho-Young Kim, Chair
Associate Professor Sung Jae Kim, Vice-Chair
Assistant Professor Rhokyun Kwak
Associate Professor Yoonchan Jeong
BK Assistant Professor Hyomin Lee

ABSTRACT

During ion concentration polarization (ICP) phenomenon, the electro-osmotic instability (EOI) was the core mechanism of electrokinetic transportation from aqueous electrolyte solutions to ion-selective membranes. The lab-on-a-chip (LOC) device based on the micro-/nano-fluidic channel enabled one to identify such flow field as well as the associated electric field and concentration profile. Recently, electrokinetic analysis considering microchannel wall charge effect has shown that surface conduction (SC) or electro-osmotic flow (EOF) played a decisive role for ion transportation while the EOI was negligible owing to the micro-size channel dimension. Hence, it is necessary for experimental verification of such mechanisms in detail. Thus, the deeply understanding of the ICP phenomenon is crucial regarding the electric field, concentration distribution and flow-field in LOC device.

In this thesis, we experimentally investigate the transporting role of surface conduction and of electroosmotic flow during ICP by effectively controlling the cross-sectional area of the PDMS microchannel structure. From the basis of our

verification, we extracted the valuable parameter (the ratio of the perimeter to the cross-sectional area of the microchannel) in the region where surface conduction dominates. The result has shown that the surface contacting the electrolyte solution becomes higher, the ion transport through the surface charge extremely increases. Thus, it is expected to be a strategy for developing the effective ion rectification in ICP platform.

In the second section of this thesis, we conceived a device design that can measure the concentration field and electric field utilizing the localized EOF inside the ion depletion zone. The fabricated groove microchannel captured the EOF of the entire ion depletion layer. Interestingly, the non-negligible diffusio-osmotic contribution were observed as well as the EOF one, which has never been predicted before. In general, diffusio-osmotic flow (DOF) was observed in either cases where the gradient of the concentration field is abrupt or the concentration is very low. The ion depletion zone generally maintains a low concentration field while causing instability of the flow field inside the ICP, which proves to be the effect of DOF. Furthermore, it is confirmed that the DOF

phenomenon occurs depending on the kind of the cation by tracking the micro-oil droplet and the mass spectrometer.

In the final section of this thesis, we presented the issue on the electrical power of the ICP system and the solution with an engineering skill. Some experiments has suggested the permanent structures (i.e. pillar arrays or spacer) or the heterogeneous membrane system. Those system have in common to control the size of the ion depletion zone with the structures. Here, we proposed the ICP system incorporated with the injection of the hydrodynamic control. This system enabled one to shrink the ion depletion zone, while the size can be determined both by the electric field and the pressure driven flows. Furthermore, the voltage-current characteristics in the ICP-pressure system was significantly different from that in the conventional ICP system, exhibiting the elimination of the limiting current. Thus, such system offered the higher electrical power conversion efficiency.

We revolutionize the LOC device not only for investigating the underlying ICP phenomenon by tracking the flows, but also for demonstrating the possible

transport mechanisms and relative physics by measuring the electrical responses in detail.

Keywords: Ion concentration polarization (ICP), Overlimiting conductance (OLC) mechanisms, Diffusio-osmosis, Hydrodynamic convection effect.

Student number: 2012-23239

CONTENTS

Chapter 1.

Introduction

1. 1 Motivation

Ion concentration polarization (ICP) is the phenomenon that the significant ion concentration gradient occurred around the ion-selective membrane when the additional electric field was applied[1]. Especially, the microscopic physics inside the ion depletion zone has been actively studied than the one inside the ion depletion zone since the ion concentration, the electric field and the electro-convections were tightly coupled during ICP[2]. Recent development of lab-on-a-chip (LoC) technology has enabled one to investigate the ion depletion zone in detail[3-8]. For example, one has successfully visualized the convective motions via fluorescent particles around the ion-selective membrane and the other one measured the electric field and concentration via implanted electrodes, etc[9]. Such revolutionized LoC platform, however, encountered the undesirable instability issues i.e. the step-wise concentration distribution or the secondary (or tertiary) convection in the middle of ion depletion zone, which needed to be

further analysis beyond the previous ICP theory. Hence, it is necessary for demonstrating the transport mechanisms and their related electrokinetic responses with the further experimentations.

1. 2 Purpose of the research

This section basically consists of three research questions based on the electrokinetic behaviors inside the ion depletion zone[10-12]. Here, the electrokinetic behaviors covered from the surface-driven ion transportation in microchannels to the non-equilibrium Debye layer structure in front of the ion-selective membrane interface. The three questions are mentioned below:

(1) Recent investigation revealed out the overlimiting conductance (OLC) related to the electrokinetic transportation in the microchannel charged wall, especially regarding the surface conduction and electro-osmotic flows[11, 13, 14]. Are there any possible ways to verify the OLC mechanisms by experimentations with an experimental measurement and with the direct observation in LoC device?

(2) Direct observation by microscopic view inside the ICP layer revealed out the unpredictable electrokinetic phenomenon such as step-wise concentration distribution or the instability therein[2, 9]. Such demonstrations was conducted with the installed electrodes, which could hinder the clear measurement during ICP. Are there any engineering skills to obtain the electrokinetic responses without implanting any obstacles (i.e. electrodes) inside the ion depletion zone?

(3) The conventional ICP system inherently involve the current limitation, which significantly lowered the power efficiency[15, 16]. The previous research have revealed out that the expanding ion depletion zone limit the ionic flux through the electrochemical membrane. Recent investigation suggested the experimental method to control the ion depletion zone by installing the permanent structure such as pillar arrays or the heterogeneous membrane[17, 18]. In practical system, however, it is much needed to control the ion depletion zone on demand for their own convenience. How can we obtain the ICP system without implanting such structures above?

Those questions above have in common that there were the general lack of

experimental studies in entire ICP system based on the LoC device[19]. Thus, we will highlight the detailed background research and the related necessity for developing the experiments in the following sections 1.3.

1. 3 Necessity of the research

This section describes the work that have been performed previously on each questions. Furthermore, the necessity of the research is also provided in terms of the general view of the ICP phenomenon and their background in detail.

(1) The ICP demonstrations and their analyses had been based on the oversimplified 1D model[20, 21]. This was true since the conventional ICP problem was used to be conducted with the large but compact device, only consisting of aqueous solution/membrane/aqueous solution. Hence, it was possible to derive the current density, only divided by the cross-sectional area of the device dimension. The active carriers in the volumetric aqueous solution were subject to the electro-osmotic instabilities in addition to the diffusion and

the drift, which was normally assumed until the discovery of charged wall geometric effects.

Due to the high surface to volume ratio, the microfluidic platform based ICP theory came into the surface driven electrokinetic responses such as surface conduction or electro-osmotic flows[6, 7, 10, 11, 13, 22]. The related physicochemical features exhibited the pre-concentration or deionization shock during ICP phenomenon. While the microfluidic platforms have been the promising tools for investigating the detailed physics, the detailed experiments considering the charged wall effect has not been conducted yet. Recently, a unified theory of OLC through an electrolyte confined within a charged microchannel has been developed in M. Z. Bazant group[11], but the direct experimental confirmation is still lacking.

Thus, we will demonstrate the OLC mechanisms in diverse aspect ratio of the surface to volume, by fixing the volume of microfluidic channels. The detailed fabrication method and the following result will be discussed in the Chapter 3. In addition, the further experiments will be presented in the high

surface aspect ratio to the volume regime (we will call this as a SC regime). By modifying the unified theory, we extract the surface to volume ratio as a parameter and fit the experimental data in line with our calculation.

(2) Recent ICP theories has predicted the complex features of the internal ion depletion zone in terms of concentration distribution, electric field and the electro-convective instabilities[4]. Especially, they revealed out the amplified electric field and lowered ion concentration therein, which was significantly different from the bulk solution (outside the ion depletion zone). Recent LoC devices offered the concentration profile *in situ* by visualizing the fluorescent Dye (i.e. Alexa 488 or FITC) or by measuring the conductance via implanted electrodes[9]. Furthermore, the placing electrode technology paved the way for the direct measurement of the electric field, which could not be presented in the conventional 2D devices.

While importance in unveiling the internal structures for advancing ICP science, the experiments reported the inherent issues such as electro-osmotic instability and the step-wise distribution inside the ion depletion zone. Those

reported has never been explored before since the previous theory predicted the monotonous decreasing concentration profile from the end of the ion depletion zone to the ion-selective membrane interface. Several seminar experimentations have still provided the secondary (or tertiary) vortex structures and their dynamics *in situ* by visualizing the fluorescent particle motions during ICP[9, 23]. However, the conventional LoC device has its own limitations for providing any insights of the complex structures since the general lack of precise experimental information far beyond the presented electrokinetic phenomenon inside the ion depletion zone.

Thus, we propose the groovy microchannel structures for capturing the high-resolution electrokinetic slip velocity profiles along the ion depletion zone[24]. In every groovy structures, the amplified electric field was localized only in a tangential direction, resulting in the electro-osmotic flows (EOF) therein. More importantly, the induced EOFs were trapped inside the structures as a form of circulating flow motions due to the coupling of EOF and the pressure driven flow from the membrane. This experimental demonstration

clarifies the entire map of electrokinetic flows inside the ion depletion zone for the first time.

The detailed fabrication method and the experimental results will be presented in Chapter 5.

(3) The ICP theories has developed the voltage-current characteristics that exhibited the ohmic-limiting-overlimiting regime[1]. This nonlinear behaviors was associated the electrokinetic phenomenon based on the diffusion, the drift and the electro-convections inside the ion depletion zone. In the meantime, the ion depletion zone has been known as the nuisance during ICP phenomenon since the low concentration therein led to the high resistance of the entire system[25]. Thus, it is necessary for overcoming the inherent power loss by the expansion of the ion depletion zone in the end.

Recent investigations has revealed out that manipulating the ion depletion zone was possible with the help of installing structures such as pillar arrays, spacers, chambers or the heterogeneous membrane system[17, 18]. Such

demonstrations in both theories and experiments could successfully control the ion depletion zone dimension, while eliminating the limiting current behavior in I-V curves. However, most previous attempts have utilized as a permanent structure so that it is impossible to tune the ohmic-limiting-overlimiting current characteristics on demand.

Thus, we proposed the conventional ICP system incorporated with the hydrodynamic flow injection method[26]. The injecting flows successfully restricted the expansion of the ion depletion zone. Furthermore, the ionic current through the shrunken ion depletion zone significantly altered to the previous voltage-current characteristics, which showed the enhancement of the current value in entire regime. While the additional pump power required to suppressing the ion depletion zone was negligible compared to the overall power consumptions, the electrical power efficiency was significantly increasing in this fluid controllable system. The detailed description will be followed in the Chapter 6 with the corresponding images and their electrical behaviors.

1. 4 Research range

The main focus of our research is to investigate the complex and coupled electrokinetics in micro-/nano-fluidic system, which electrokinetic phenomenon is called as ion concentration polarization (ICP). Since the ion transportation in ICP system is mainly determined by the physicochemical hydrodynamics inside the ion depletion zone, it is crucial to clarify the concentration profile, electric field and the electro-convection therein. Thus, we demonstrated such important features in LoC by conceiving the idea, fabricating the devices and conducting the observation/electrical measurement/data analysis.

1. 5 Definitions of terms

Since the complex terminology in the field of ICP, we defined several new terms in advance in order to give the clear information to the thesis reader.

Ion concentration polarization is the phenomenon that ion concentration imbalances between the ion-selective membrane when the electric field was applied. ICP phenomenon happens in every aqueous solution / membrane /

aqueous solution system, but the interesting physicochemical dynamics occurred only near to the ion-selective membrane around the dimension of 1mm.

Ion-selective membrane is assumed to be a fluid-impermeable, but an ion-permeable system. In this thesis, Nafion resin is used to an ion-selective membrane and it additionally possessed the highly-negative surface charge density.

Ion depletion zone represented the low concentration region adjacent to the ion-selective membrane. In this thesis, the anodic side of the Nafion membrane corresponds to the ion depletion zone since the cations only can penetrate the Nafion and the remaining anions were repelled for satisfying electro-neutrality.

Limiting current comes from the classical theory that only considered the diffusion and the drift around a hundred years ago. The value can be derived by Nernst-Planck equations. While the recent electrokinetic studies investigated the overlimiting conductance regime above the limiting current value, the limiting current can be the guide line for the ICP theory. For example, the hydrodynamic convections induced by the electric field can be found far above the limiting

current.

Overlimiting conductance (OLC) is normally referred to an additional ion transportation in the voltage-current characteristics. This can be characterized as a combination of the exponential *I-V* function to the linearized conductance. This is the representative nonlinear characteristics during ICP. The OLC is mainly attributed to an additional ion transportation by the appearance of the electro-osmotic instability.

Electro-osmotic instability (EOI) occurs when the tangential electric field inside the extended space charge (ESC) layer make up for the high electric field in normal direction to the ion-selective membrane. Since the EOI acts as an ion-delivering mechanism from the neutral bulk into the membrane, the EOI contributes the OLC when it comes to the OLC regime.

Surface conduction (SC) and electro-osmotic flows (EOF) are also identified as an ion-transporting roles in in the porous media or in microchannel. Due to the high surface to volume ratio in such system, the surface driven electrokinetic transportation has been highlighted in the field of ICP. Recent

theory suggested their electrokinetic role in terms of *I-V* characteristics.

1. 6 Thesis overview

In this thesis, the underlying physics and the microscopic electrokinetic features of ICP (resulting from the micro- and nano-channel interface) phenomenon are investigated and used to (1) demonstrate the overlimiting current (OLC) mechanisms for extracting the valuable parameter, (2) demonstrate the extended space charge (ESC) layer with the flow controllable device and (3) capturing the critical roles of diffusio-osmotic flows in the ion depletion zone for the possible applications.

The thesis is broken down into 7 chapters as follows.

In Chapter 1 and Chapter 2, the background and motivation were presented and a brief review of relevant nanofluidic transport phenomena is discussed.

In Chapter 3 and Chapter 4, we investigated the overlimiting conductance (OLC) mechanisms of the geometrical varieties by correlating between the flow

topology and the electrical responses. In addition to this, we extracted the valuable parameter (ratio of the cross-sectional area of the microchannel to the perimeter) in SC regime.

Chapter 5 presented the non-negligible roles of diffusio-osmotic flow inside the ion depletion zone. The main contribution of this work is to design the groovy microstructures in the microchannels, which successfully localized and captured the EOF. Interestingly, the non-negligible diffusio-osmotic contribution were observed as well as the EOF one, which has never been predicted before. The assumption that the cation-shell striping provided the step-wise mobility distribution, resulting in the sudden drop of concentration profile therein.

In Chapter 6, we experimentally demonstrated the voltage-current behaviors in the presence of the additional convective flows adjacent to the Nafion membrane systems. The ion depletion zone can be controlled by the several flow conditions, exhibiting the significantly shrunken structures in front of the Nafion membrane. The voltage-current characteristics was significantly tuned in the entire flow conditions, resulting in the enhancement of the electrical

power consumptions in the entire ohmic-limiting-overlimiting regime.

Chapter 7 concluded the remark of the thesis and mentioned the potential future work stemming from the presented work.

In Appendix, we will present the chronopotentiometric measurement in a shear-flow assisted ICP system. This electrochemical method has the implication to investigate the further ICP studies such as the extended space charge layer or the overlimiting current mechanism in detail.

Chapter 2

Research Background

2.1. Perm-selectivity of the nanochannel

Electrical double layer

The free ions in the electrolyte solutions are redistributed depending on the charged walls[27]. For example, the co-ions of the surface charge were expelled from the surface while the counter-ions were extracted toward the surface. Such tendency leads to forming an electrical double layer (EDL), which consisted of (1) the Stern layer that was compactly attached to the surface and (2) the diffuse layer that the free ions were located.

This interesting nature has been independently developed by both Louis Georges Gouy in 1910 and David Leonard Chapman in 1913[28]. The “Gouy-Chapman model” significantly improved the complete pictures of the ion redistribution as a function of distance from the charged surface, adopting the Boltzmann statistics with an electrostatics. Once the counter-ions were attracted and fixed at the surface with the potential ψ_s, the ions were immobile in this layer

(as known as Stern layer). The Stern layer have the zeta potential ζ, other than the charged wall as shown in Figure 1. The diffusive actions of free ions by Brownian motion could lead to the spatial distribution in the diffuse layer. Thus, the EDL thickness is characterized by Debye screening length (λ_D) as

$$\lambda_D = \left(\frac{\varepsilon_0 \varepsilon_d RT}{F^2 z^2 c_0} \right)^{0.5}$$

, where ε_0 is the permittivity of air, ε_d the permittivity of water, R is the gas constant, T the absolute temperature, F the Faraday constant, z the valence of ionic species and c_0 the molar concentration in the electro-neutral solution.

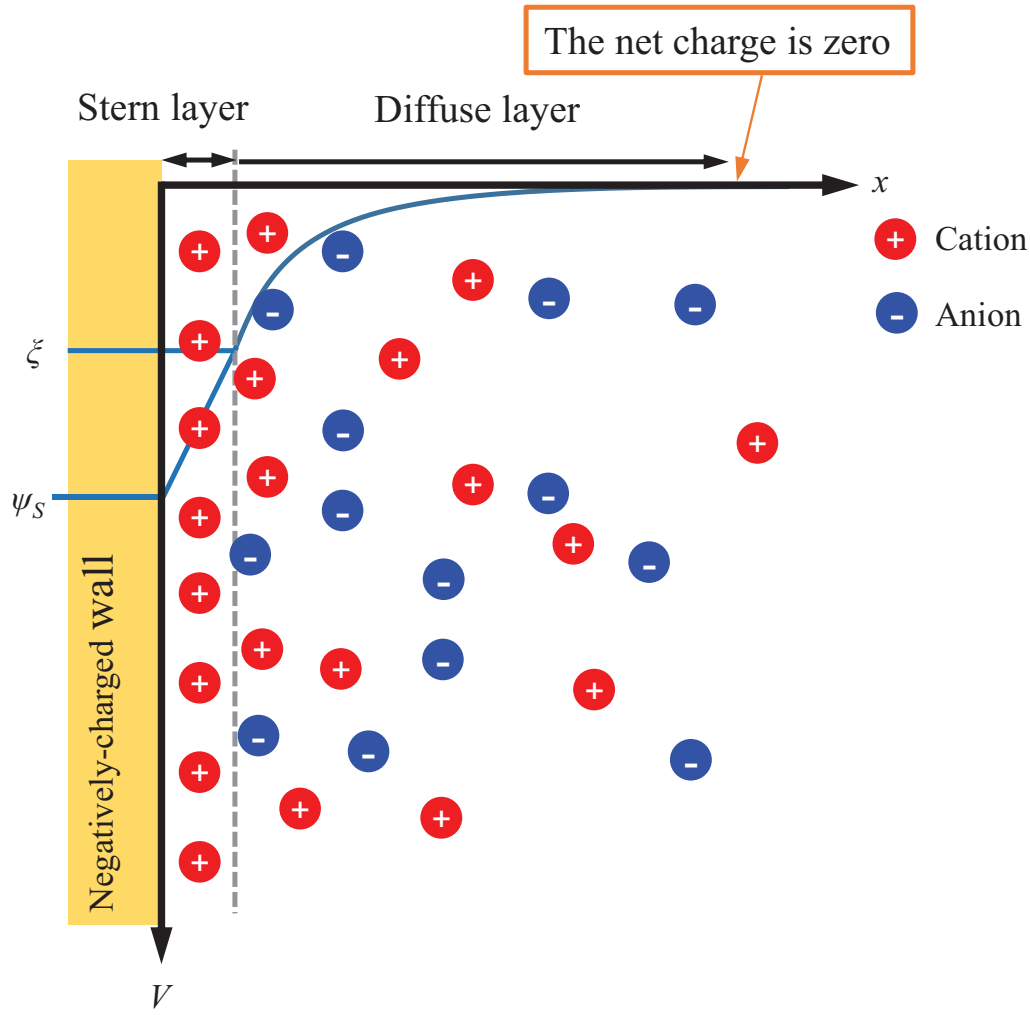

Figure 1. Schematics of the electrical double layer formation.

Electrical double layer overlap in nanofluidic geometry

When the fluidic system becomes enough small as the few nanometers size, the electrical potential in the center of the nanochannel remained relatively high as shown in Figure 2[29]. This is normally referred to the EDL overlap. Hence, the nanofluidic geometry showed the specific-charge selective nature. For example, when the nanofluidic channel possessed the negative charge surface, only the positive ions can penetrated from the bulk electrolyte into the nanochannels while the positive ions cannot due to the electrostatic repulsion. This is the fundamental basis of the electrochemical membrane systems for water purification and fuel-cells[3, 19, 30, 31].

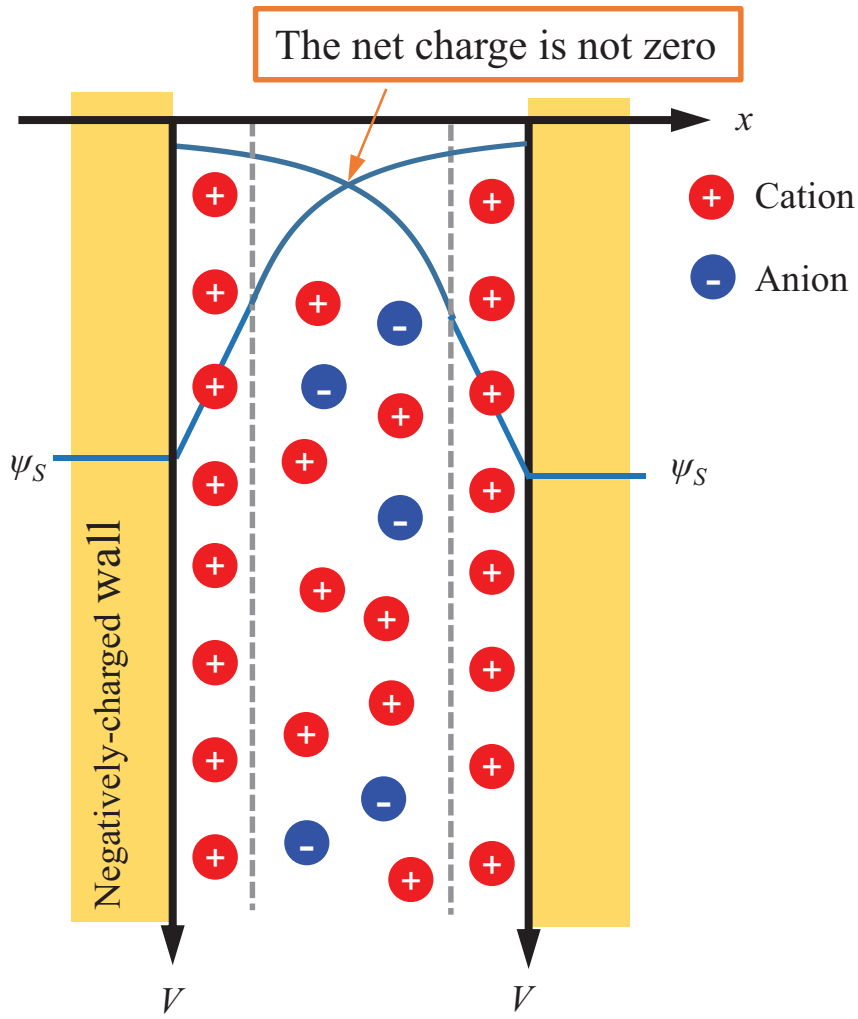

Figure 2. Illustrations of the EDL overlap inside the nanofluidic geometry. Once the nanochannel dimension (L_{nano}) becomes enough small to $L_{nano} < \lambda_D$, the EDL was overlapped in the middle. Thus, the electroneutrality breaks down therein.

2.2. Ion Concentration Polarization (ICP)

When an electric field is applied from the bulk electrolyte solution into the cation-selective nanochannel, the electrokinetic transport of both signs of ions is superimposed on the diffusion and drift in the bulk electrolyte[1, 20]. At the selective membrane interface, however, the cations are solely penetrated toward the nanochannel while the anions were remained due to the selectivity[32, 33]. The left-behind anions then were repelled from the membrane toward the bulk reservoir in order to satisfy the electro-neutrality. Thus, the ion depletion zone was formed at the anodic side of the membrane. In the other side of the electrochemical membrane, the anions were attracted toward the membrane with the same reason, forming an ion enrichment as shown in Figure 3 (a). Thus, the significant ion concentration gradient around the cation-selective membrane drove the ion concentration polarization (ICP) phenomenon as shown in Figure 3(b)[4].

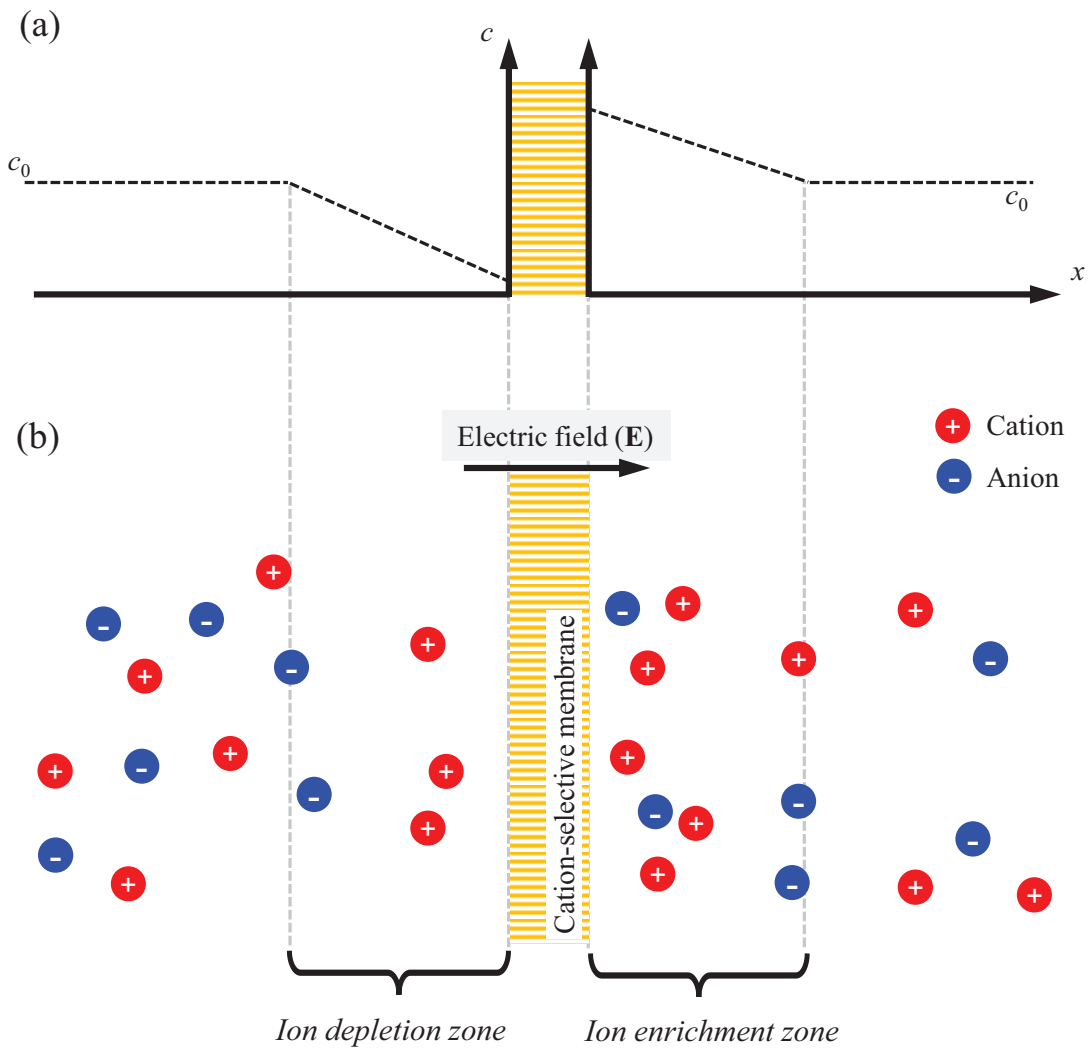

Figure 3. Schematics of ICP configuration with (a) a concentration profile and (b) the ion distributions around the cation-exchange membrane.

2.3. Limiting current and space charge modulation

Limiting current

When the ion penetration into the membrane equals the ion supply from the bulk membrane, the concentration at the interface reaches zero at the steady state. The concept of maximum ionic flux, which is called a "limiting current" was first introduced by Nernst a century ago as shown in Figure 4[34]. The classical system was describe by the Nersnt-Planck equations as

$$\frac{d}{dx}\left(D_{+}\frac{dC_{+}}{dx} + \mu_{+}z_{+}FC_{+}\frac{d\phi}{dx}\right) = 0 \quad \text{and}$$

$$\frac{d}{dx}\left(D_{-}\frac{dC_{-}}{dx} + \mu_{-}z_{-}FC_{-}\frac{d\phi}{dx}\right) = 0$$

, where F is the Faraday's constant (a mole of charge), $z_{\pm}$, $\mu_{\pm}$, $C_{\pm}$ and $D_{\pm}$ are the valence, mobilities, concentration of each ions and diffusivities of each ionic species, respectively.

Assuming that the system size is L with the boundary conditions, $C_{+} = C_{-} = C_0$ and $\phi = \phi_0$ at $x = L$, the limiting current can be derived as

$$I_{\mathbf{lim}} = \frac{zFDC_0}{L} \quad \ldots(4)$$

, where $z_{+} = z_{-} = z$, $D_{+} = D_{-} = D$ and $\mu_{+} = \mu_{-} = \mu$.

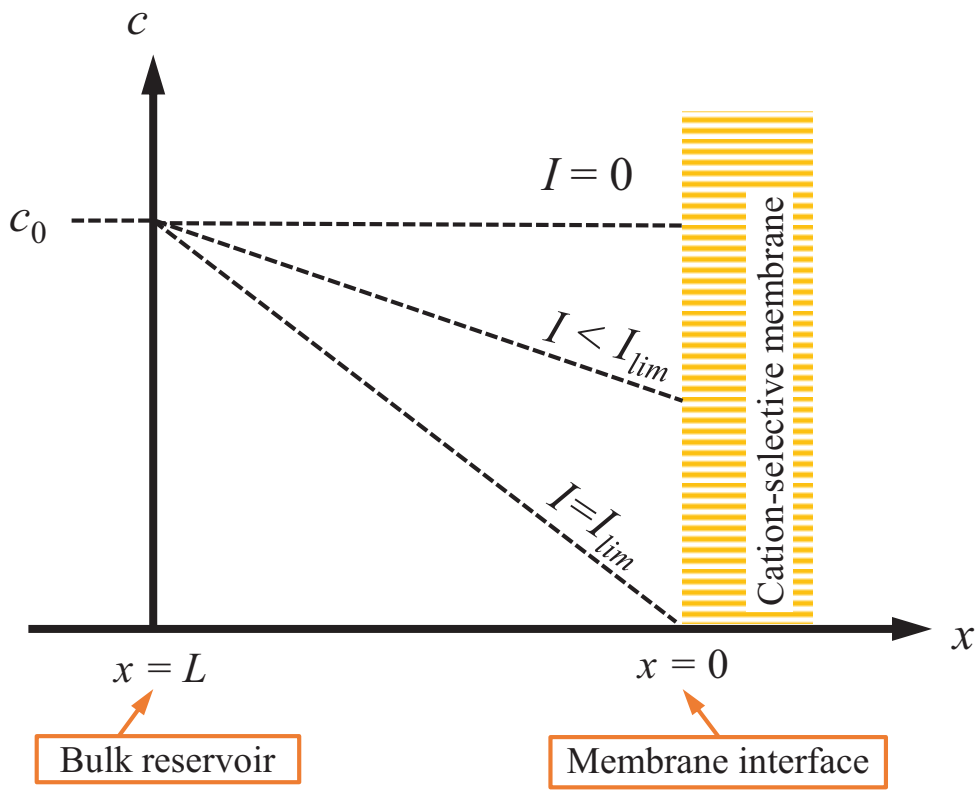

Figure 4. Illustration of concentration distributions in the cation-selective membrane systems under the current level at $I = 0$, $I < I_{lim}$ and $I = I_{lim}$.

Electro-neutrality breakdown around limiting current

The classical postulations described the ionic current in the bulk electrolyte where the quasi-neutrality meets, thus the space charge were neglected in the earlier time. In 1962, Levich first noticed the breakdown of electroneutrality

around the limiting current, yielding the approximate solutions via Poisson-Nernst-Plnack (PNP) equations[28, 35]. Since the charge density of the EDL exceeds the salt concentration at the interface, the eventual event has been poorly expected over the limiting current. This paradox was first resolved by Smyrl and Newman in 1967, who suggested the double layer expands at the limiting current as the Poisson-Boltzmann[36, 37].

Extended space charge (ESC) layer

At 1978, Rubinstein and Shtilman pointed out that the non-equilibrium "space charge" existed far above the classical limiting current, significantly extending toward the neutral as shown in Figure 5[20, 38-41]. This new structure is not a part of a stretched (or distorted) EDL, rather it is an extended vicinity of the counterions concentration minimum when co-ions expelled therein by electric field. The analytical solutions from the asymptotic matches of mathematics revealed out the anomalously large electric fields and charge densities, compared to the equilibrium EDL at small currents. The extended space charge (ESC) layer

can be found not only in fluidic systems containing cation-(or anion-) exchange membrane, but also in the micro-batteries and electrochemical systems such as fuel cells.

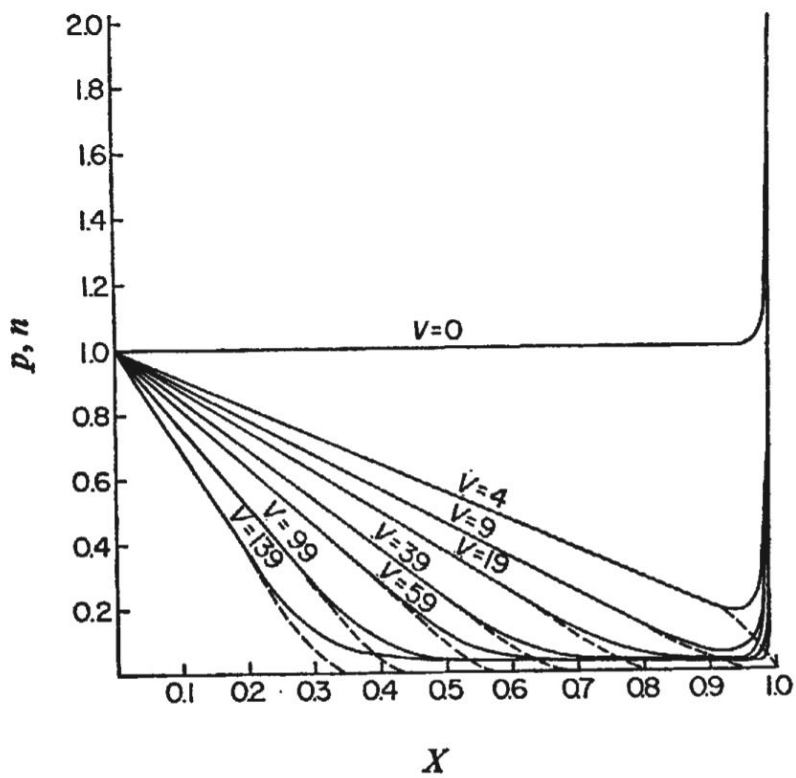

Figure 5. Simulation results from the Reference [20], illustrating the non-equilibrium space charge existed in the electroneutral bulk far beyond the limiting current values.

Electro-osmotic slip in cation-exchange membrane

With the development of the ESC layer at larger current level, Rubinstein and Zaltzman expected the electrostatic body force as a slip boundary condition for the adjacent electroneutral bulk[42, 43]. Resolving all the boundary layer in entire system, the linear hydrodynamic stability of the quiescent concentration polarization was shown in a diffusion layer. This system mainly consisted of the convective Nernst-Planck equations for the ionic concentrations and electric potential, coupled with a singularly perturbed Poisson equation (with a screening Debye layer, the ratio of the system dimension to the EDL size) and the Stokes equations[11]. These analysis played a key role in explaining the electro-convection in the electrochemical membrane systems and was able to describe the transport mechanism above the limiting current.

The electro-convective systems in electrochemical membrane systems were normally compared to the Rayleigh-Benard convection as shown in Figure 6 since the convective formation during temperature gradient possessed the flow-slip condition in tangential direction at the hot plate interfaces.

Figure 6. The comparison illustration of electro-convection and the Rayleigh-Benard convection. They exhibited the instabilities in each cation-selective interface and the hot-plate.

2.4. Overlimiting conductance (OLC)

Combined with the diffusion and drift, electro-convection during ICP played a deterministic role for ion transportation from the bulk diffuse boundary into the ion-selective membrane[1, 5, 11, 43]. The direct numerical simulations considering Poisson equation (for electric potential), Nernst-Planck equations (for ion concentration) and Navier-stokes equations (for fluid flows) predicted the additional ion transport above the limiting current value, which is named after overlimiting conductance (OLC) as shown in Figure 7. The classical theory only considered the diffusion and drift failed to predict the OLC due to (1) ignoring the space charge of the EDL and (2) underestimating the effect of the electro-convection. This peculiar and unique voltage-current characteristics is a fingerprint of ion-selective surface such as electrodes or electrochemical membranes[21, 22, 24].

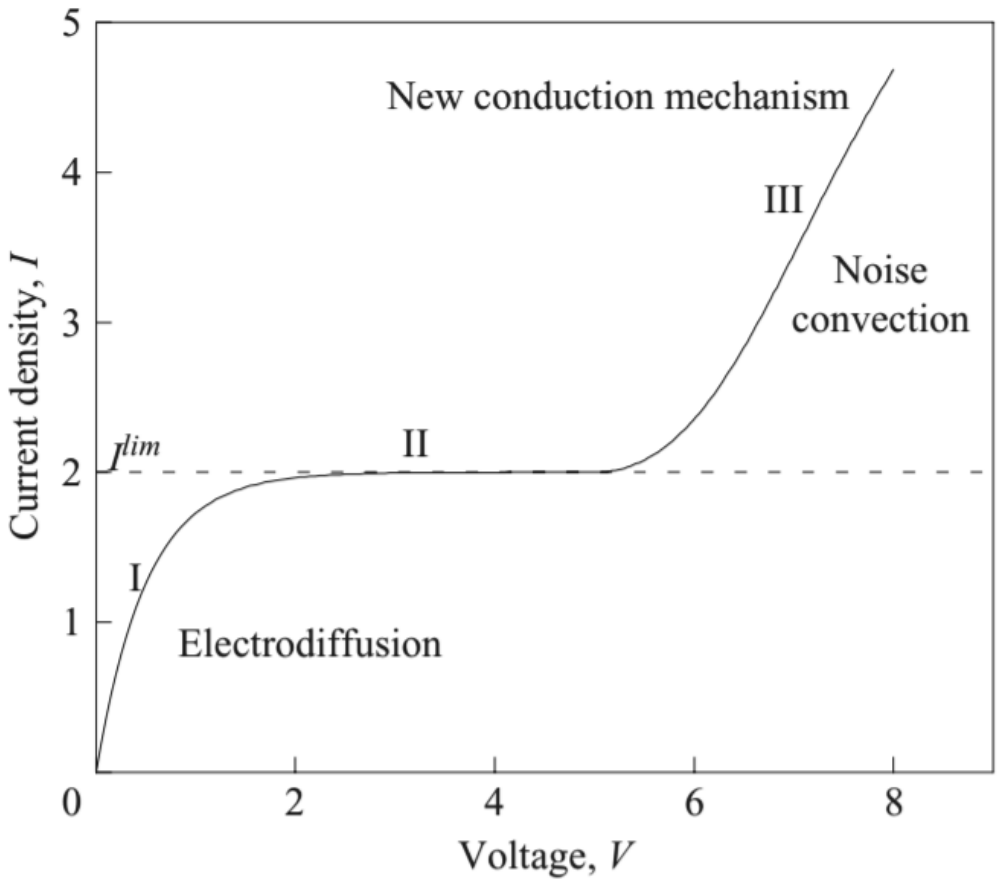

Figure 7. The simulation result of voltage-current characteristics considering both the space charge and the electro-convection in addition to the classical postulations (drift and diffusion). This figure was adopted from the reference [43].

2.5. ICP phenomenon in Lab-on-a-Chip device

Charged sidewall effects on OLC

Recent investigation of the ICP experiments has been conducted on the lab-on-a-chip devices, which enables one to demonstrate the underlying physics in detail[44]. The numerical simulations also has been made for understanding the geometrical confinement effects[11, 22, 45, 46]. Figure 8 depicted the Dydek's postulations of the effects of the charged wall on OLC, suggesting that (1) the surface conduction (SC) dominates in narrow channels and (2) convection by electro-osmotic flows (EOF) on the sidewalls dominates for larger channels. Such theoretical work gives a clear insight into the electrokinetic phenomena in microchannels, while emphasizing the different OLC mechanisms from the wider (or unsupported) channels[47-50].

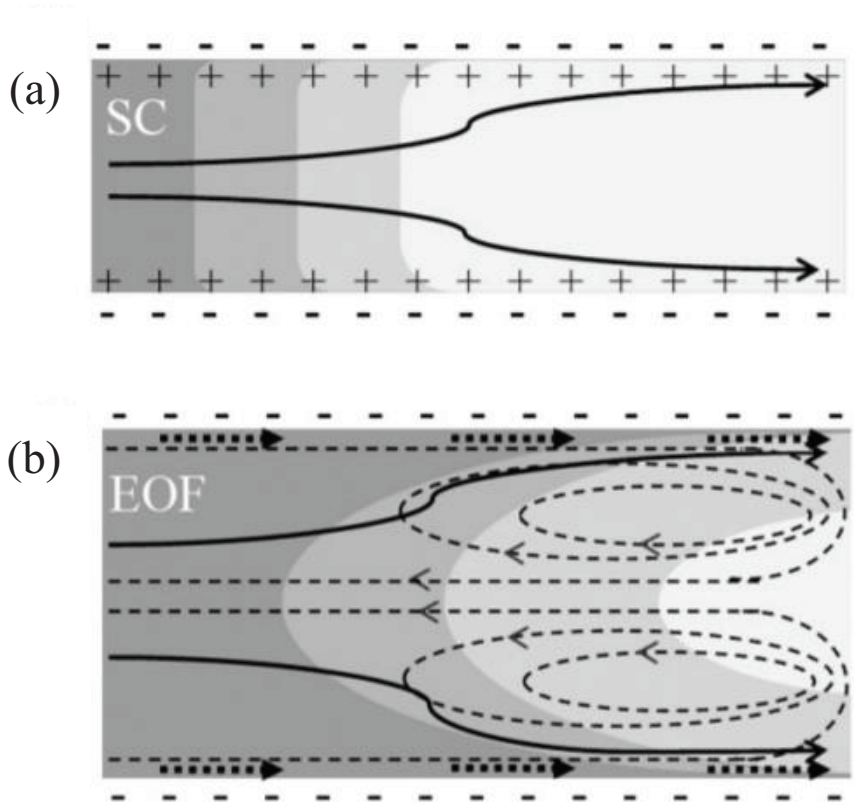

Figure 8. Physical picture of overlimiting current in a microchannel. The current is carried primarily by (a) surface conduction (SC) and (b) electro-osmotic flow (EOF). This figure was adopted from Ref [11].

Deionization shock in microchannel

Normally, ion transportation in charged surface such as microfluidic devices and porous media exhibited two forms as bulk conduction (the conduction of the neutral bulk solution) and surface conduction (the conduction of excess ions in the EDL)[8, 10, 51, 52]. When it comes to the systems involving the ion-selective membrane, there exists a “deionization shock” from the cation-selective membrane toward the microstructures as shown in Figure 9. This nonlinear dynamics are possible due to the electrodynamic behaviors of both cations and anions. While cations was attracted to the negatively charged walls and repelled from the membrane while anions were escaping from both from the membrane and charged surface. Thus, the negative charge molecules (including ions and particles) were pushed toward the bulk coupling with the nonlinear dynamics from the membrane and the EOF. This interesting phenomena provided the promising directions for the ICP-related applications such as biological sample preconcentration and seawater desalination[30, 53].

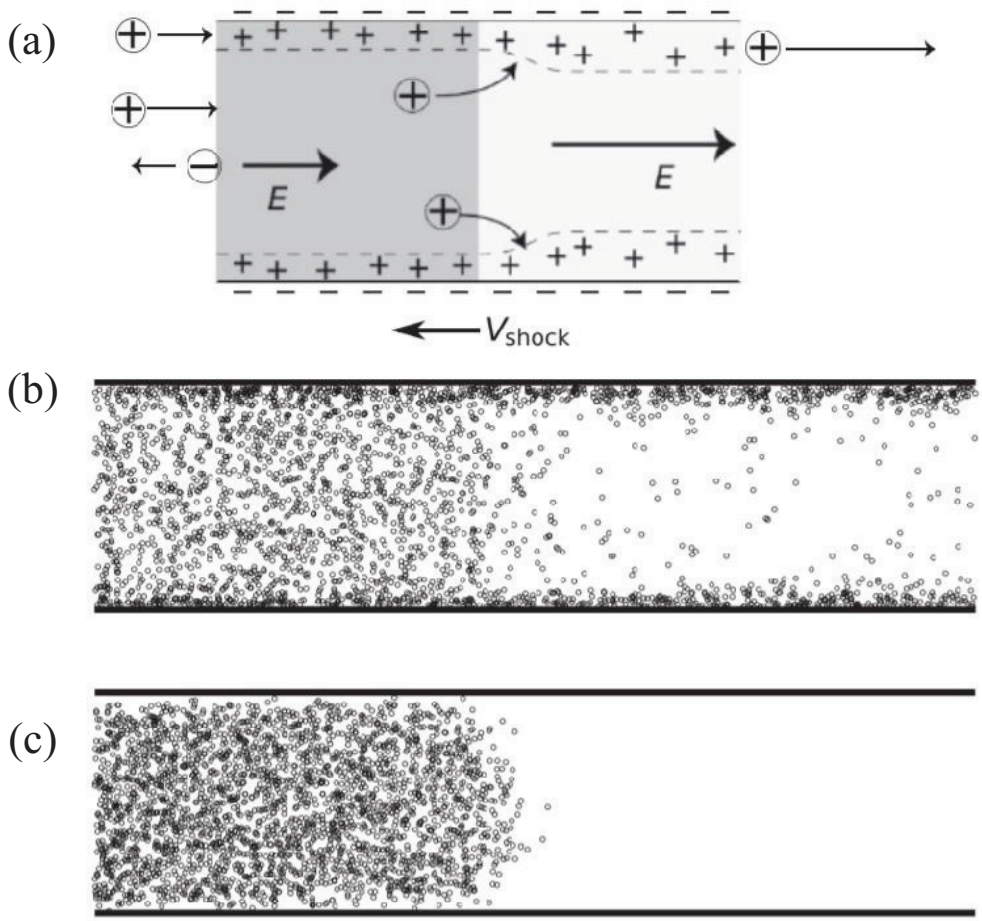

Figure 9. (a) The sketch of ion fluxes in a microchannel with negatively charged walls. (b) The ionic current flows of cations dominates in the EDL while (c) the anions remained in the bulk. This figure was adopted from Ref[8].

2.6. Relevant applications

Desalination

The repulsion of charged ions from the ion depletion zone gives the opportunity for the novel desalination process[2, 3]. Even though the additional pressure was applied from the opposite direction of the deionization shock, the salt concentration maintained low near the cation-selective membrane. This enabled one to develop the ICP desalination process, converting the seawater (salinity ~ 500mM or 30,000mgL^{-1}) of the continuous stream into the fresh water (salinity < 10mM or 600 mgL^{-1}) during operation as shown in Figure 10. Such remarkable approaches pave the way for the great advances in the engineering applications of ICP.

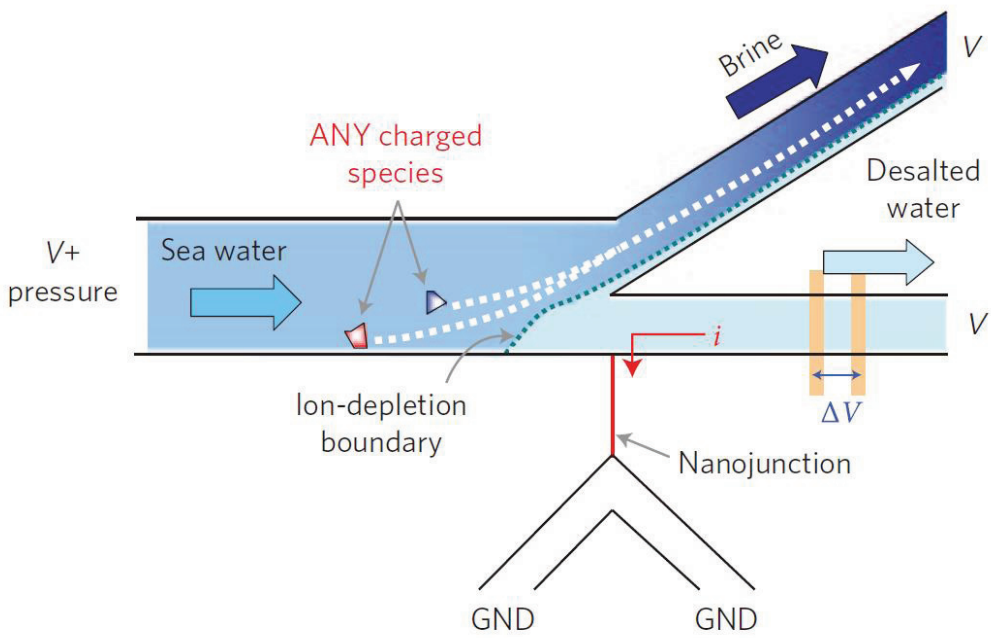

Figure 10. The schematics of ICP desalination. The electrokinetic operations associated with the external pressure field. This figure was adopted from Ref[3].

Separation of charged species

The base operation was same as the desalination process, but the removal target during ICP desalination was somewhat difference. This separation method applied to the charged molecules such as microorganism, biomolecules as shown in Figure 11 (a)-(c)[4, 29, 54]. This ICP-based elimination method has the potential for the engineering advances in the electrochemical membrane systems.

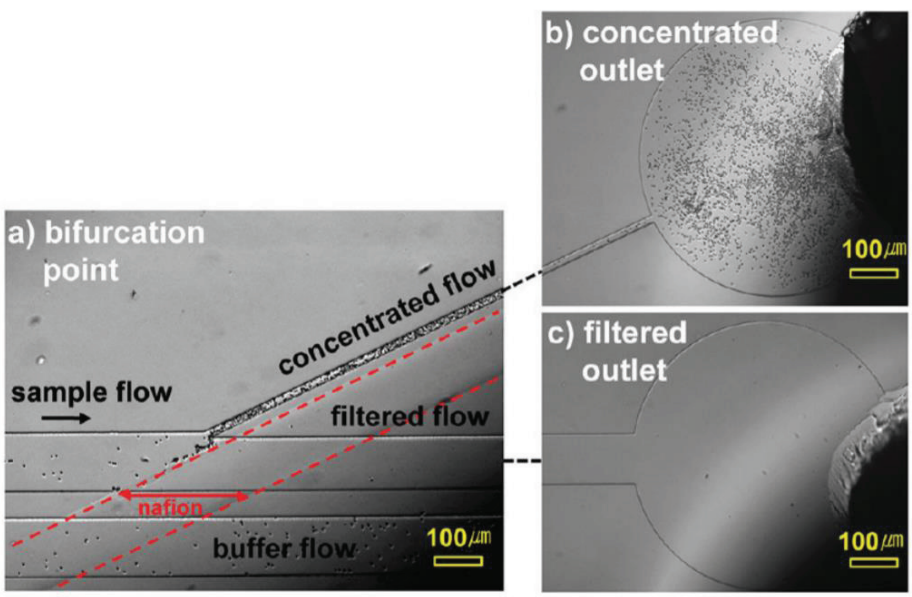

Figure 11. A continuous-flow concentrator for red blood cells. (a) the operating images of the concentrator and the comparison images of the outlet of (b) concentrated flow and (c) filtered flow. This Figures was from Ref [xx].

Preconcentration and separation

The preconcentration process occurred during ICP due to the combination of the charged species repulsion from the ion depletion zone and the electro-osmotic flows from the neutral bulk[55-58]. Such preconcentration can be modulated with the species diffusivity rather than the salt concentration of the bulk. In our group, the selective preconcentration has been validated with two difference dyes in the aqueous solutions[59]. Figure 12 showed the operations based on the preconcentration plug extractions using the pneumatic valve. Benefited from the work, one can develop the targeted bio-molecule extractions from the mixture in the aqueous solutions on demand, while the ICP-based LOC can be utilized as a tool-set for developing numerous engineering applications.

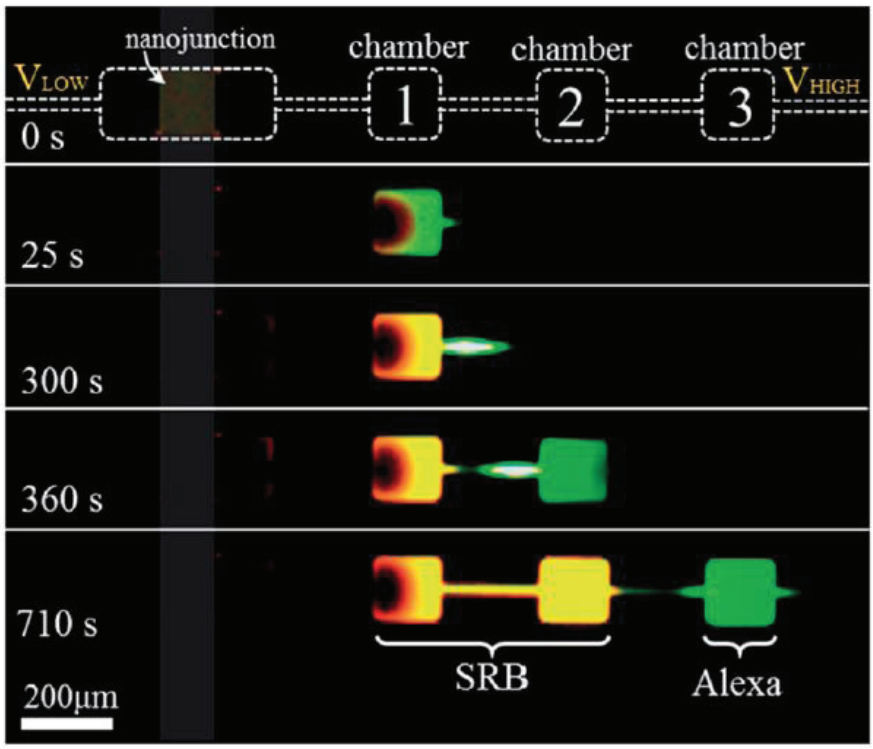

Figure 12. Time-lapse images of selective preconcentration of different fluorescent dyes with SRB and Alexa. High concentration ratio was represented by the brightness of fluorescence. This Figure was adopted from the reference [59].

Chapter 3

Experimental verification of surface conduction and electro-osmotic flows in microchannels

This chapter consists is the basis for a paper which has been published to Physical Review Letters in 2015[45] and benefited from editing and directing from Sungmin Nam, Prof. Martin Z. Bazant and Prof. Sung Jae Kim. For the developing the micro-/nano-fluidic device, Dr. Joonseong Heo, Prof. Geunbae Lim, Dr. Jaesuk Moon and Prof. Gun Yong Sung have gave us the valuable comments. In this work, Sungmin Nam and I prepared all the devices and conducted experiments. We demonstrated the all the OLC mechanisms by both SC and EOF, using the in-situ visualization of flow-field and the direct measurement of voltage-current relation. While he captured the particle motions therein, I obtained the OLCs of those systems.

3.1 Introduction

Over the past decade, electrokinetic phenomena in nanoscale fluidic channels

have drawn significant attention, for both fundamental theory and novel engineering applications [3, 4, 60, 61]. Much progress has been made in understanding electro-convection during ion concentration polarization due to electro-osmotic flows near the membrane or nanochannel interface driving salt depletion [15, 62]. Due to the complexity of direct numerical simulation of the Poisson equation (for electric potential), Nernst-Planck equations (for ion concentrations) and Navier-Stokes equations (for fluid flows) in multi-dimensional geometries [38-40], as well as inherent limitations of the classical dilute solution model [29], it is crucial to directly observe in particle motion and flow fields in precisely controlled micro/nanofluidic geometries [63, 64].

Recent experimental investigations based on the micro/nanofluidic platform reveal complex electrokinetic phenomena in microchannels near an ion perm-selective membrane or nanochannel junctions, which cannot be described by one-dimensional diffusion-drift equations. The classical theory of ion concentration polarization (ICP) predicts a constant concentration gradient in the quasi-neutral electrolyte and saturation of the current to the Nernst diffusion-

limited value at high voltage [28]. The key features of steady ICP under direct current are as follows. (1) In case of cation selective membrane, the electrolyte concentration at the anodic side of the membrane is strongly depleted within ICP layer and approaches zero at the membrane at the limiting current [65]. (2) Due to the low salt concentration, the electrical conductivity zone significantly decreases, leading to a greatly amplified local electric field [2]. (3) The large electric field drives fast electrokinetic flow inside the depletion zone leading to strong vortices in order to satisfy the continuity conditions [1, 16]. (4) The strongest vortex at the membrane leads to secondary vortices to form multiple concentration zones inside the depletion zone, providing inherent instability issues [9, 42, 66]. (5) The limiting current and over-limiting conductance can be adjusted by manipulating the strong convection [18, 25]. Since the ion depletion zone expands with the strong convection, suppressing the convection can reduce the total electrical resistance of the system, although this trend depends on the voltage and geometry (since electro-convection clearly lowers the resistance close to the limiting current and compensates for the reduced conductivity). (6)

The salt concentration during ICP in microchannels tends to form very sharp gradients between the depleted and concentrated regions, perhaps first observed a decade ago [33]. In micro/nano/micro-channel junctions, where steady over-limiting current has been observed [23], salt gradients propagate as shock waves, [6, 12][28] or ``deionization shocks" [30-32] at constant current, due to the nonlinear effect of ion transport in the electric double layers of the sidewalls. These observations suggest that multiple transport mechanisms may be involved when over-limiting current occurs under strong confinement.

A unified theory of over-limiting conductance through an electrolyte confined within a charged microchannel has recently been developed [22], but direct experimental confirmation is still lacking. The theory predicts a transition between two new mechanisms, surface conduction (SC) and electro-osmotic flow (EOF) that dominate in nanochannels and microchannels, respectively. The EOF mechanism is driven by large electro-osmotic slip in the depleted region on the sidewalls (not the membrane at the end of the channel) [34], leading to "wall fingers" of salt transported by vortices faster than transverse

diffusion [22,35]. This new mode surface convection thus cannot be described by classical Taylor-Aris dispersion [34,35]. The EOF mechanism, extended for "eddy fingers" in a random porous medium, has been confirmed indirectly by experiments measuring the current-voltage relation, scalings with salt concentration and surface charge, and desalination efficiency of "shock electrodialysis" [36]. The SC mechanism has also been confirmed in straight nanopores with controlled surface charge by again predicting the current-voltage relation and by *ex situ* imaging of metal electrodeposits grown along the pore walls by surface conduction [37].

In this letter, we provide the first *in situ* observation of the SC and EOF mechanisms and the predicted geometrical transition between them. The motion of fluorescent tracer particles is visualized to reveal the internal dynamics in both regimes. The over-limiting conductance is also measured, and the predicted scalings with channel depth are confirmed, including a maximum that had escaped notice at the critical thickness of the transition.

3.2 Experimental setup

Micro-nanofluidic devices are fabricated in PDMS as shown in Figure 13. Current is driven in aqueous KCl 1mM solution through a cation perm-selective Nafion nanojunction to generate ICP. Under the experimental conditions, the surface charge of the microchannel is negative. Each device has the same bulk microchannel conductance by fixing the cross-sectional area as the depth is varied, since the resistivity of bulk electrolyte is linearly proportional to the area. The physical dimensions are shown in Table 1. According to the theory [22], using typical surface charge in water, the dominant mechanism of overlimiting current mechanism should vary with the microchannel depth between surface conduction for d<2um, electro-osmotic surface convection for 2um<d<20um, and electro-osmotic instability on the membrane for d>20um. The quasi-steady current-voltage relation is measured by linear sweep voltammetry with a slow sweep rate, as in Ref. [36].

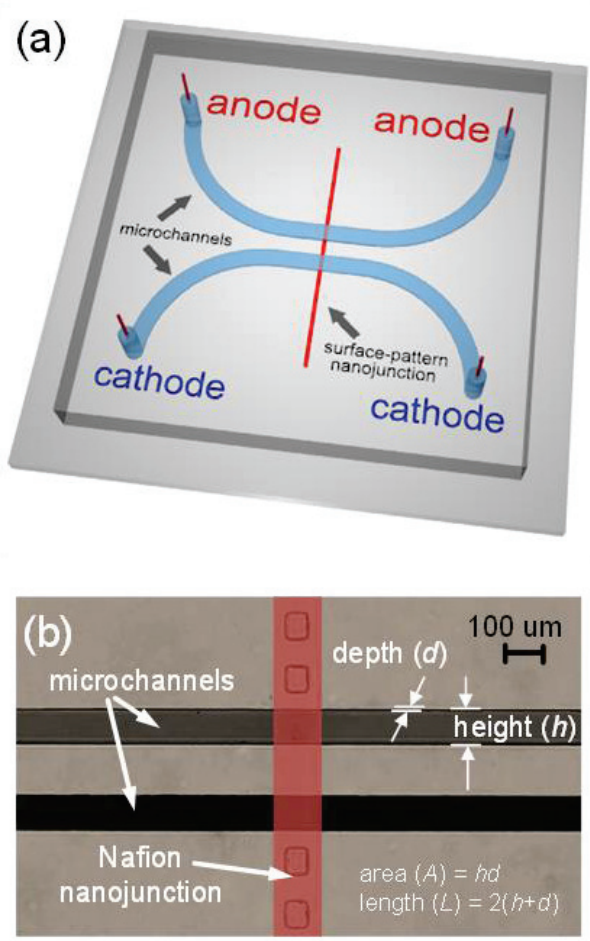

Figure 1. Schematic diagrams of (a) H-shaped micro/nanofluidic device and (b) microscope image of the device. External electric voltages are applied at two north reservoirs, while two south reservoirs are electrically grounded. The depth (d) and height (h) are varying to obtain different cross-sectional area ($A=hd$) and unit boundary length ($L=2(h+d)$).

d (μm)	h (μm)	$Area$ (μm^2)	L (μm)
2	210	420	424
5	84	420	178
6.5	60	390	133
11	38	418	98
14.5	30	435	89
18	23	414	82
22	20	440	84

Table 1. Physical dimensions of micro/nanofluidic device of the same cross-sectional area.

3.3 Result and Discussion

Below the limiting current, as expected, the current-voltage relations of the mirochannels with different depths all collapse onto a linear relationship, as shown in Figure 2, indicated by “range (i)”. The curves of 2um, 6.5um, 14.5um and 22um are only shown for the graphical simplicity. We refer to this as the “Ohmic region” since there is a constant apparent conductivity for steady electro-diffusion, even though both diffusion and electromigration of the cations contribute to the total flux [9]. As the salt concentration approaches zero at the

membrane interface, the classical diffusion limited current is reached, as indicated by “range (ii)” in the Figure 14. As the applied voltage increases further, another region of over-limiting current with a smaller, constant conductance is observed (range (iii)), whose physical origin should be determined. The trend with depth is qualitatively similar to the theoretical predictions [22]. For the thinnest channel (2um), the limiting current range is almost missing, and the over-limiting conductance (slope) is larger than for all the larger depths. Moreover, the 2um depth leads to the largest over-limiting current, since it has the largest are to volume ratio, and thus the greatest effect of the new surface transport mechanisms.

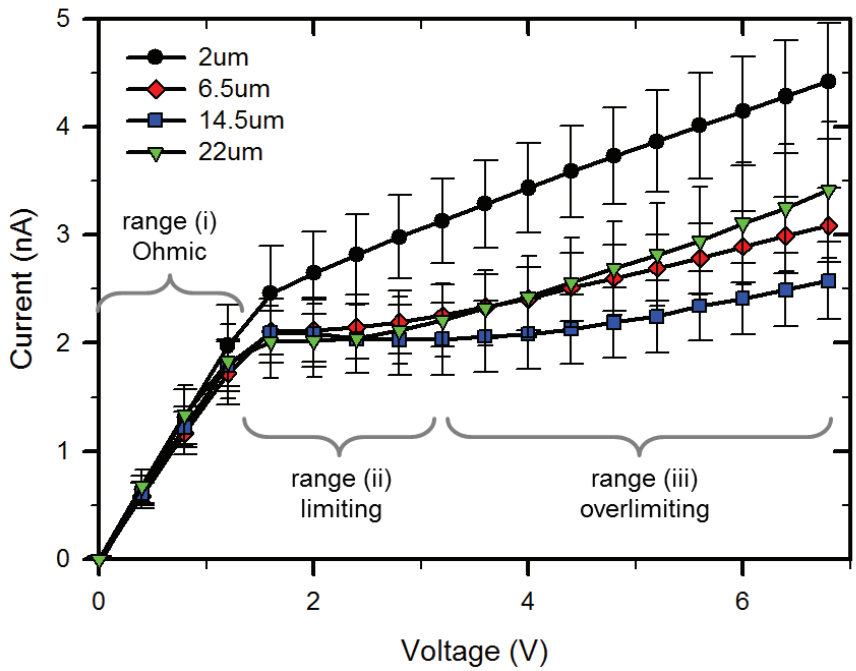

Figure 14. A current-voltage plot for micro/nanofluidic device consists of varying *h* and *d*, but the identical cross-sectional area so that the microchannel conductance keeps being the same. Thus, Ohmic currents are mostly the same, while limiting and overlimiting current values are significantly different. Voltage is swept at 0.2V/15sec. Each line is measured at least 10 times for guarantee a repeatability.

In order to extract a quantitative conclusions, the overlimiting conductance for each depth is obtained by least-squares fitting of the slope of the data in range (iii) and plotted in log-log scale as shown in Figure 3. The error bars increase in the deeper microchannels due to the flow instability, as clarified in the inset of Figure 15. While previous studies have established the simple power-law scalings of over-limiting conductance with salt concentration and surface charge in a fixed geometry [36,37], our data reveal a non-monotonic dependence on the microchannel depth with a minimum conductance at a depth of roughly 8um. Although this non-trivial behavior is predicted by theory [22,36], it has not been considered before. In nanochannels, the over-limiting conductance due to surface conduction is proportional to the volume/area ratio, or inverse depth, d^{-1}, which decreases with increasing depth. In contrast, the over-limiting conductance due to electro-osmotic surface convection in microchannels is predicted to have the opposite trend, scaling as $d^{4/5}$. Although the 4/5 exponent follows from subtle scaling arguments [22,36], the increasing conductance with increasing depth can be easily understood as a result of larger vortices carrying more convective flux.

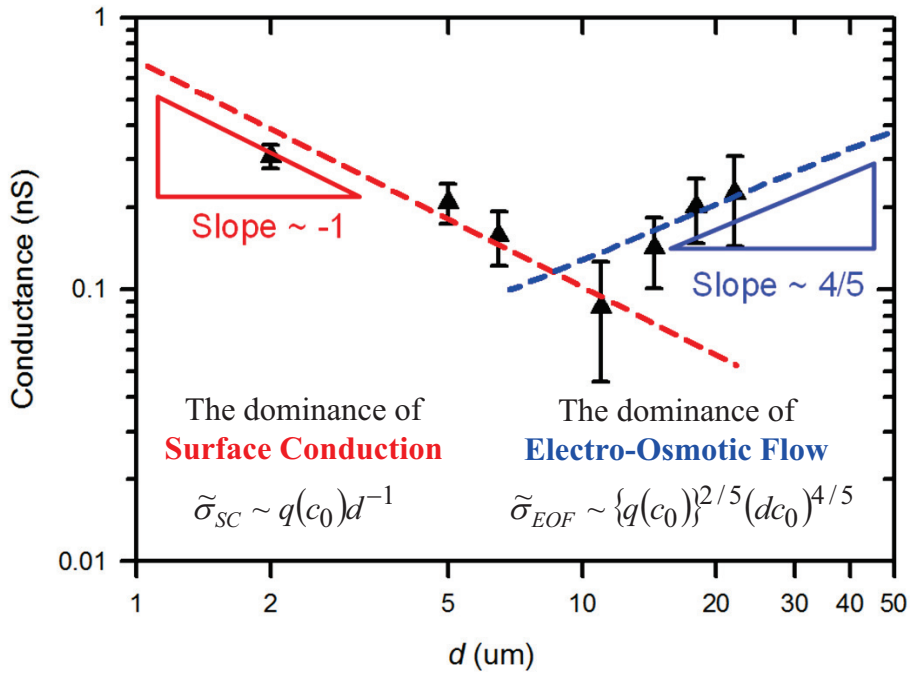

Figure 15. A overlimiting conductance plot as a function of the depth of microchannel in log-log scale. Linear scaled plot is shown in inset. It clearly shows the transition of the surface conduction governed regime ($\propto 1/H$) to the electro-convection governed regime ($\propto$H^(4/5)).

The theoretical scalings are consistent in Figure 3. The decreasing d^{-1} scaling for the smaller nanochannels is clear from the data and supports the surface conduction theory. The increasing $d^{4/5}$ scaling for electro-osmotic flow is also consistent with the data for the larger microchannels as a possible limiting scaling law, although the data is not conclusive. Remarkably, however, the minimum conductance around d=8um [22] is identical to the theoretical prediction of the critical depth from the intersection of the two scaling laws.

In order to correlate the scaling transition in overlimiting conductance with the existence of electro-convection, the electrokinetic flows are imaged during the current-voltage measurement, and their snapshots are shown in Figure 16. Each column has the same depth, and each row represents the time-evolution of the flow field. Note that the scale bar in the first column is different from others since 2um deep device has larger region of interest than others. The electrolyte contains a fluorescent dye and microparticles to track both concentration and flow fields, respectively. The length of depletion zone is also tracked by the dye, and it presumably represents the thickness of diffusive layer.

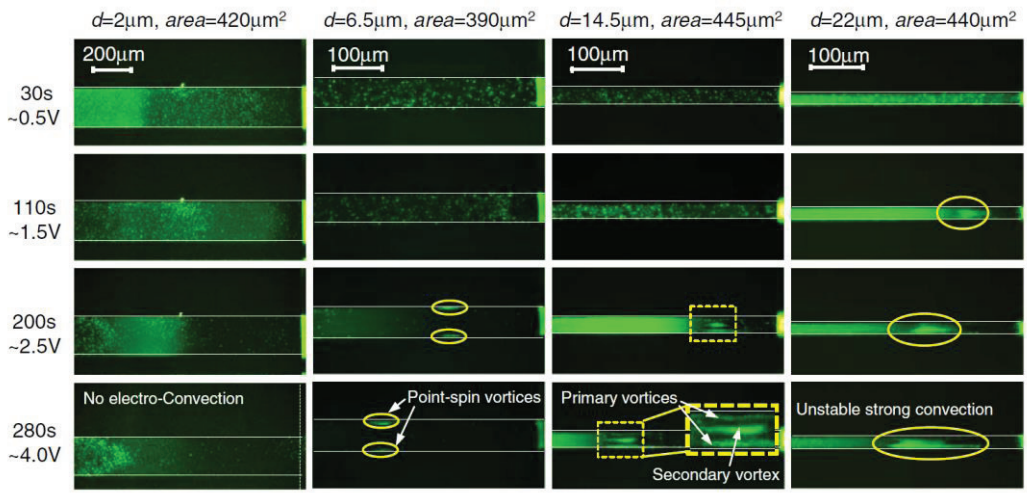

Figure 16. Microscopic images of flow tracking by fluorescent dye and particles. Each image is taken at a given time (or voltage) as noted. Note that the scale bars are different. Shallower depth effectively suppresses an electro-convective flow than deeper one. At *d*=14.5um, the convective flow at top and bottom creates a secondary vortical flow at the stagnation point in the middle of channel. Over *d*=22um, the flow finally becomes unstable.

As shown in the fourth row of the Figure 16, electrokinetic flows are significantly different and changed as a function of the depth of the microchannel, as clearly seen in the supporting videos for each depth. At 2um depth, a flat depletion zone propagates as a deionization shock wave from the nanojunction over the microchannel [1, 67], and the strong vortical motions are largely suppressed and hardly observed because of geometrical constrictions [12,23]. Transverse diffusion of the dye across the depth also eliminates concentration gradients [22,35]. Closer to the transition depth (8um), a pair of point-like weak vortices are initiated at the top/bottom of microchannel in case of 6.5um deep microchannel, especially after the limiting current range (>2.5V). As the depth increases to 14.5um, the vortices are strengthen and become the primary convections at the side of microchannel, while they induce secondary vortices at the stagnation point in the middle of the microchannel, leading to a strong electro-convective flow [9]. Finally, the electro-convection becomes very strong and unstable in case of the 22um deep microchannel, thus approaching the bulk behavior [28-32]. Combining the results of the overlimiting

conductance measurement and the flow field tracking (*e.g.* the transition from the surface conduction governed regime to the electro-convection governed regime), we can suggest that the mechanism of overlimiting current behavior cannot be attributed solely to surface conduction or electro-osmotic surface or bulk convection. Instead, each phenomenon plays an important role and dominates in different micro/nanochannel geometries.

3.4 Conclusions

In summary, we experimentally demonstrate the competition between different transport mechanisms for overlimiting current in microchannels by fixing (or changing) the conductance. With the microscopic imaging of electrokinetic flow and electrochemical measurements, we can separate the effects of the electro-osmotic flow and surface conduction depending on the geometrical confinement. Consistent with the theory [22], surface conduction dominates in nanochannels and electro-osmotic surface convection in microchannels with a minimum conductance at the predicted transition around 8um depth A clear understanding

about the mechanism of the overlimiting current would be essential not only for scientific fundamentals but also furnishing effective engineering strategies to exploit and control ICP (and the overlimiting current) in electrochemical systems such as fuel cells, batteries [31], electro-desalination systems [3, 68, 69], and template-assisted electrodeposition [37].

Chapter 4

Surface conduction in a microchannel: developing the micro-/nano-fluidic diodes using current rectification

This chapter consists is the basis for a paper which is in preparation for the journal publications. In this work, Seoyun Sohn conducted the electrical measurements and obtained the conductance information. Inhee Cho fabricated all the micro-/nano-fluidic geometries including geometry design. Both of them also contributed to the development of analytical solutions for the 3-dimensional surface conduction models, verifying the obtained conductance. They also did the write the manuscripts of the paper. Prof. Hyomin Lee and Prof. Sung Jae Kim benefited the paper directions and gave the scientific information.

4.1 Introduction

Being represented by the Nernst-Planck equation, the classical theory to elucidate ion transportations through aqueous solution involves the contribution of diffusion, drift and convection[28, 70, 71]. While numerous experimental

and theoretical studies have been conducted using the equation so far, recent findings that have been accelerated by the advances of micro/nanofluidic research teach us that there are additional significant mechanisms beyond the equation[8, 11, 14, 19, 24, 43, 45, 72, 73]; electroosmotic instability (EOI), electroosmotic flow (EOF), surface conduction (SC) and diffusioosmosis. Among them, the electrokinetic operation at SC regime affords versatile utilities in micro/nanofluidic platforms especially due to its stability. Such platforms with extremely high surface to volume ratio allow the surface effect to predominate over the volume (or bulk) conduction which has been mainly considered in the classical Nernst-Planck equation. SC is defined as the flow of excess charges in an electrical double layer (EDL) formed near a charged surface[11]. There are two major factors that determine the regime of ionic current; (i) the characteristic length scale and (ii) the surface charge density of the substrate. Smaller length and higher surface charge density drive the system to surface effect-dominant regime, *i.e*. SC regime. While seminal theoretical characterization of SC has been widely applied for stable electrokinetic

operations or enhancing system conductance[13, 14, 52, 74, 75], the analysis has been carried based on two-dimensional approximation which inevitably requires at least one infinitely long axis. When a system has a confined geometry such as practical micro/nanofluidic devices, the third axis, which has been neglected in two-dimensional approximation, should be considered.

In this letter, therefore, we experimentally investigated the three-dimensional geometric effect on SC by employing a micro/nanofluidic platform that consists of two microchannels connected with Nafion nanojunction. The aspect ratios of the microchannel cross-section were designed to be varied from 0.003 to 1 so that the conductance was measured from an approximated two-dimensional limit to a three-dimensional geometry. As a function of only microchannel depth, the measured conductance values were out of theoretically predicted range, especially when the aspect ratio approaches to 1. Alternatively, the third dimensionality was included in the calculation of a volume density of fixed charges so that the perimeter to area ratio of microchannel cross-section was extracted as a single parameter to fit all of conductance data. The parameter

would be utilized as a significant design rule for various micro/nanofluidic devices such as power-efficient desalination device, highly sensitive electrical (bio-)sensors, diagnostics tools or ionic circuit components.

4.2 Experimental setup

The device we employed in this letter is shown in Figure 17 (a). PDMS-glass bonded micro/nanofluidics devices were fabricated using standard soft-lithography[76] for microchannels and surface patterning for Nafion nanojunction[77]. See supporting information for detailed device fabrication process. Figure 17 (b) gives a magnified view near the nanojunction. Two microchannels (main (red) and buffer (blue)) were connected by patterned Nafion bridge. Air-valves were installed at the side microchannels for the easiness of experimental labors and obtaining the identical electrokinetic responses with a 1-dimensional micro-nano-microchannel device by eliminating disturbances from uncontrolled hydraulic pressure[78]. Such practical devices inevitably possess a three-dimensional constriction as shown

in the inset of Figure 17 (a), imposing a critical limitation on two-dimensional analysis. In order to explore their electrokinetic properties, one of geometrical factors should be kept in constant and, in this work, the cross-sectional area ($A = dw$) of main microchannel was designed to keep the Ohmic conductance (σ_{Ohm}) constant in each design. The design parameters (width (w) and depth (d)) of main microchannel were listed in the first and the second column of Table 2. While A remained constant, the perimeter ($L = 2(d+w)$) of the main microchannel was varied accordingly. Consequently, in that aspect, one would be able to obtain a variation of L/A, perimeter to cross-sectional area ratio. It is the parameter of interest in this study in that it represents the variation of L at constant A, *i.e.* the surface conduction effect without the consideration of the Ohmic conduction. Five sets of devices whose A's were doubled from the previous set were fabricated for further investigation over the wide range of L/A.

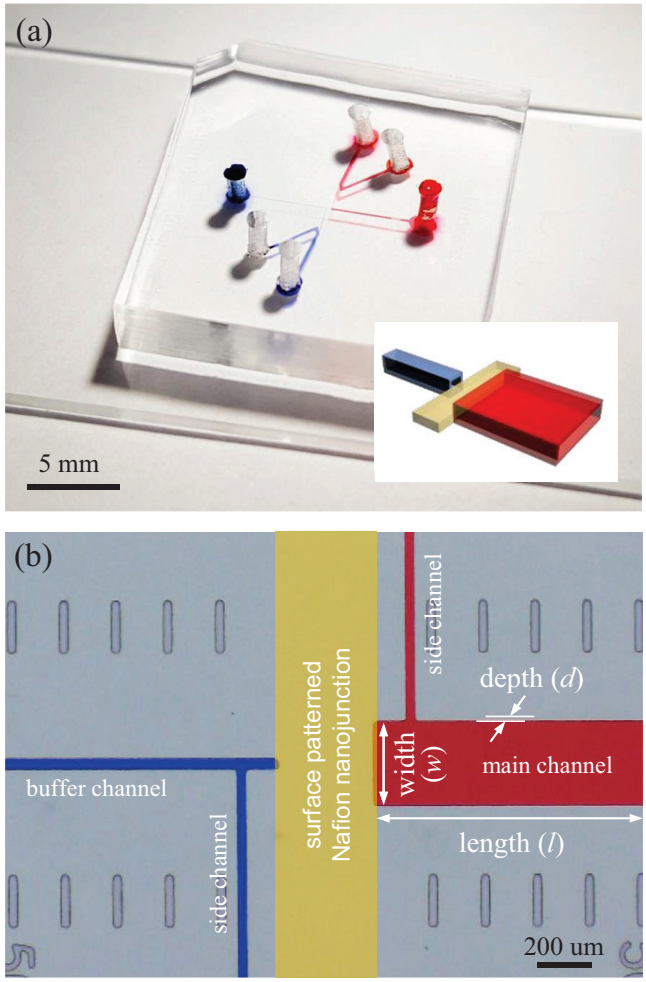

Figure 17. (a) Image of assembled device. The inset shows its schematic view of essential components near the nanoporous junction. (b) Microscopic image of the device. Two microchannels with different L/A are connected by surface-patterned Nafion nanojunction. Main and buffer microchannels are depicted in red and blue, respectively.

d [um]	w [um]	A [um^2] $=dw$	L [um] $=2(d+w)$	L/A [um^{-1}]
3	70		146	0.70
5	42		94	0.45
7	30	210	72	0.34
10.5	20		61	0.29
15	14		58	0.28
3	140		286	0.68
5	84		178	0.42
7	60	420	132	0.31
10.5	40		101	0.24
15	28		86	0.20
3	280		566	0.67
5	168		346	0.41
7	120	840	252	0.30
10.5	80		181	0.22
15	56		142	0.17
3	560		1126	0.67
5	336		682	0.41
7	240	1680	492	0.29
10.5	160		341	0.20
15	112		254	0.15
3	1120		2246	0.67
5	672		1354	0.40
7	480	3360	972	0.29
10.5	320		661	0.20
15	224		478	0.14

Table 2. Physical dimensions of all microchannels used in this work.

4.3 Result and discussion

The current-voltage relations of all dimensions listed in Table 2 are plotted in Figure 2(a)-2(c). See the supporting information for all data sets. The voltage was swept at 0.2 V/30 sec from 0-4 V. As expected, the slopes in the voltage range of 0-0.6 V (σ_{Ohm}) were almost overlapped because A was constant in each plot in Figure 18 (a). The same scenario was applied to Figure 18 (b) and Figure 18 (c) as well. Statistical analysis showed that σ_{Ohm} was roughly proportional to A as shown in Figure 2(d). More importantly, the overlimiting conductance (σ_{OLC}) was significantly altered depending on d in each plot in Figure 18 (a) - (c). σ_{OLC} is the fingerprint of electrokinetic property within micro/nanofluidic devices or nanoporous membrane system, describing additional current increment followed by the Ohmic regime and limiting current regime[1, 41, 62]. It can be extracted by reading the slope of I-V curve at a lager voltage substantially away from the Ohmic regime. The remarkable observation is that higher L/A resulted in higher σ_{OLC} even under the same A. This means that one has to fully assess the three-dimensional structure (w, d, and l).

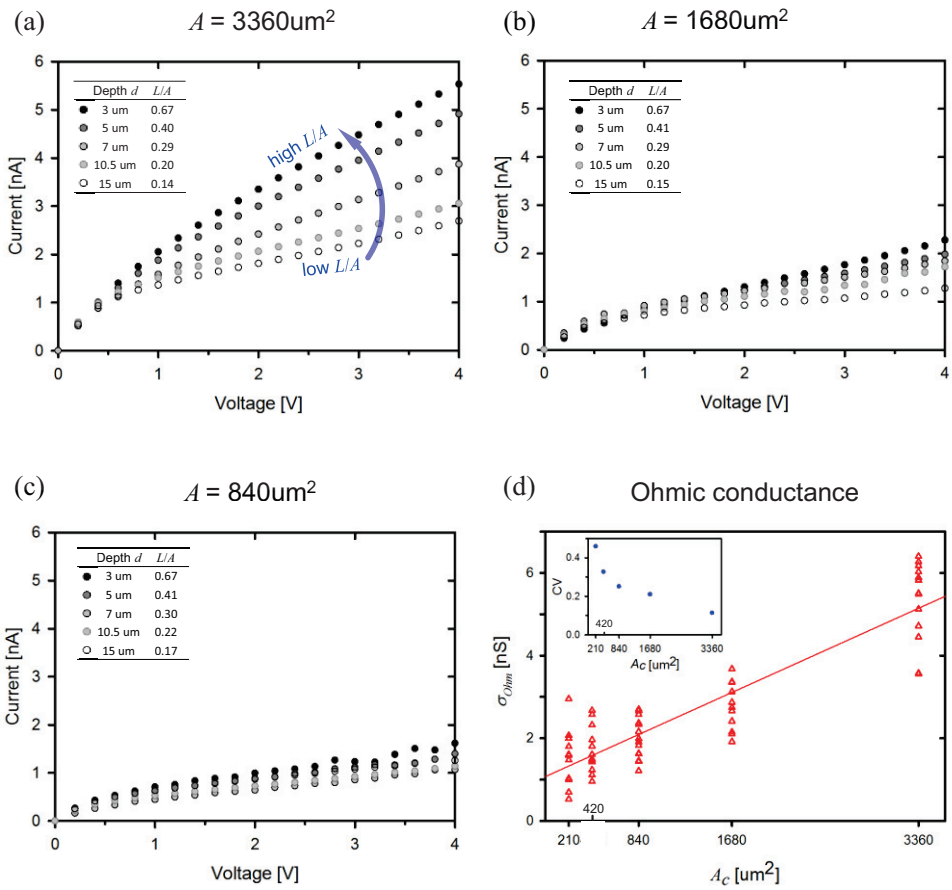

Figure 18. *I-V* responses of the devices with the microchannel cross-sectional area of (a) 3360 um^2 (b) 1680 um^2 and (c) 840 um^2, respectively. In each graph, current value increases with *L*/*A* beyond the Ohmic regime. Comparing (a) to (b) and (b) to (c), larger cross-sectional area results in higher current. (d) Ohmic conductance increases proportional to *A*.

In order to investigate the effect of dimensionality on σ_{OLC}, previously reported two-dimensional analysis and our three-dimensional analysis were conducted and the results were shown in Figure 19 (a) and Figure 19 (b), respectively. The schematics of dimensionality are depicted in the insets of each plot. The conventional two-dimensional relation[11, 14, 45], $\sigma_{OLC} = -\frac{zeD}{lkT}\left(\frac{2\sigma_s}{d}\right)$ was held in the case of extremely thin microchannel whose *z*-directional length could be considered as an infinity compared to the *y*-directional length (see red circles and line in Figure 19 (a)). In this equation, σ_s, *z*, *e*, *D*, *k* and *T* are the surface charge of material, valence of ion, elementary charge, diffusion coefficient, Boltzmann constant and absolute temperature, respectively. σ_s/d represents a surface charge contribution of a charged wall at distance *d*. The value of *l* was selected as O(1) mm. However, the exponent of *d* deviated from -1 as the shape of microchannel cross-section became a square whose *z*-directional length is now comparable to the *y*-directional length. Therefore, the full understanding of three-dimensional constriction should be required to setup the appropriate design strategy of an efficient

micro/nanofluidic device or nanoporous membrane system whose electrical performance is predominantly determined by σ_{OLC}.

Here we considered the third-dimensional constriction along z-axis as shown in the inset of Figure 19 (b). Starting from the Nernst-Planck equation in a negatively-charged long microchannel (d and w << l) with thin EDL approximation (λ_D << d and w, where λ_D is the Debye screening length), the excess charge is expressed as ρ_v/e where ρ_v is the volume density of fixed charge. While the two-dimensional analysis employed ρ_v as $\frac{\sigma_s}{zec_0}\frac{2}{d}$ where c_0 the reservoir concentration[11], here the three-dimensional constriction provided ρ_v as $\frac{\sigma_s}{zec_0}\left(\frac{2}{d}+\frac{2}{w}\right)$ which included the surface charged effects from all enclosed walls under the assumption that the edge effect at the corners of microchannel was negligible. Since the ionic flux (j) is proportional to $\rho_v V$ in the SC regime, σ_{OLC} (= j/V) should be $-\frac{ze\sigma_s D}{lkT}\left(\frac{2}{d}+\frac{2}{w}\right)$ where the last multiplier, $\frac{2(d+w)}{dw}$, corresponds to the L/A in this work. Note that this three-dimensional equation is also applicable in two-dimensional analysis as w approaches infinity.

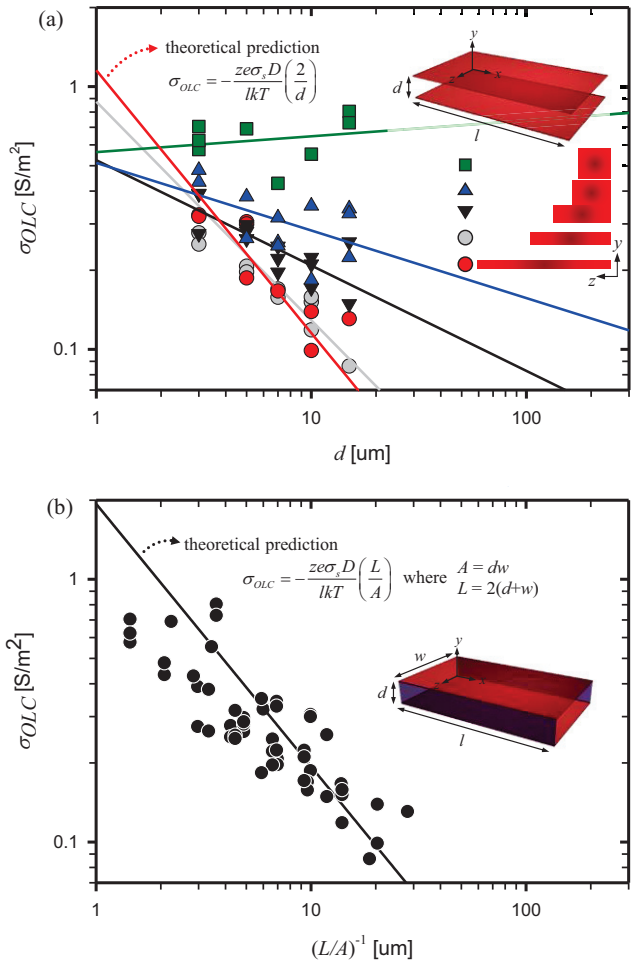

Figure 19. OLC as a function of (a) depth or (b) L/A. In (a), data points are inline with the theoretical prediction only when the z-directional length is larger enough than y-directional length (See the red circles and line). In (b), all data are well-agreed with the modified theoretical prediction as a function of $(L/A)^{-1}$, regardless of the z- and y-directional length.

All data points from Figure 19 (a) were rearranged as a function of $(L/A)^{-1}$ as shown in Figure 19 (b). The data was well-agreed with the theoretical prediction so that we can conclude that L/A is the unified parameter that governs OLC in a microchannel where SC is major current transportation mechanism. It implied that the combination of various L and A would convey an adjustable conductance so that this analysis would play a deterministic role for designing a micro/nanofluidic device or a membrane system. For example, the compartmentalization of macrochannel (*i.e.* increase L with fixed A) would provide superior conductance and stability for realizing a high-throughput massive parallel micro/nanofluidic devices [8, 13, 52, 56]. In the meantime, one can manipulate the ionic current in a stretchable or deformable micro/nanofluidics [79-81] (*i.e.* increase A with fixed L or adjust both A and L, respectively) at one's discretion for developing efficient electrical sensors or diagnostics tools. For the simplest demonstration, two microchannels of different L (*i.e.* different SC) with constant A (*i.e.* constant σ_{Ohm}) were connected by Nafion nanojunction for realizing a micro/nanofluidic diode[53,

75, 82-84] by this strategy. We choose the microchannel dimensions as in the schematics of Figure 20 (a) and Figure 20 (b) and successfully obtained the rectification factor of 1.81 and 8.41, respectively. According to our analysis, the rectification factor could be strategically manipulated with a designed L/A.

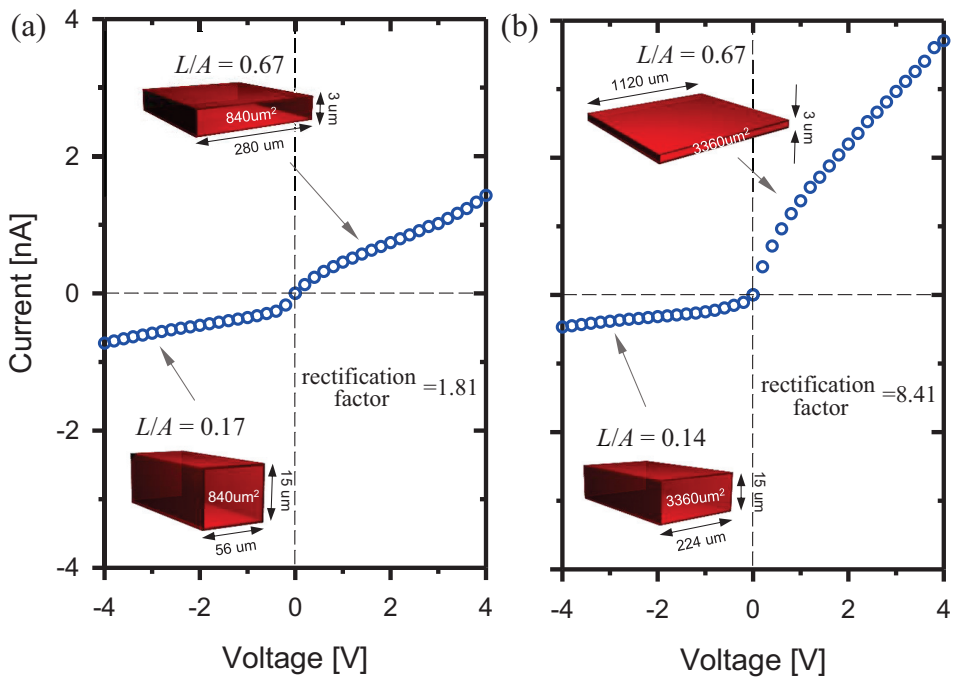

Figure 20. Current rectifications came from asymmetric L/A value of the forward and the reverse microchannel. Physical dimensions of main and buffer microchannels are as depicted.

4. 4 Conclusions

In conclusion, since a two-dimensional analysis has inherent limitations from the assumption of an infinite axis, here we present a rigorous three-dimensional analysis of surface conductive ion transportation through a microchannel. By employing a micro/nanofluidic device that had various geometrical variations, the unified parameter of $L/A = 2(d+w)/dw$ was extracted and it successfully fits to all of OLC data which had been largely deviated from two-dimensional analysis. Lastly, a simple micro/nanofluidic diode was demonstrated by proper choices of L/A. The strategy would rejuvenate the robustness of surface conductive ion transportation mechanism in a practical micro/nanofluidic device or nanoporous membrane system.

Chapter 5

Non-negligible diffusioosmosis inside an ion concentration polarization layer

This chapter consists is the basis for a paper which has been submitted to Physical Review Letters in 2016[24] and benefited from editing and directing from Dr. Wonseok Kim, Prof. Hyomin Lee and Prof. Sung Jae Kim. In this work, Inhee Cho demonstrated the ICP experiments with a groovy microstructure and visualized the captured oil-droplet. Dr. Wonseok Kim extracted and analyzed the ICP solution samples by developing a novel channel design. Prof. Hyomin Lee conducted the simulations and conceived the diffusio-osmotic contributions therein. Junsuk Kim assisted in capturing the microgroovy structure in different channel width. Prof. Ho-Young Kim gave the scientific information for the paper.

5.1 Introduction

With the aid of recent development of nano-technology, the fundamental studies of electrokinetics with the micro/nanofluidic interface have been actively

reported both on the fundamental theories and engineering applications [29, 85, 86]. One of the most exciting features in the nanoscale electrokinetics is an ion concentration polarization (ICP) phenomenon which described the significant concentration gradient formed at the both ends of the nanochannel (or nanoporous membrane) under dc bias [1, 12, 28, 62]. Several seminal experimental/theoretical works have reported on the underlying physicochemical hydrodynamics inside ICP layer. Especially, the in-depth understanding of an ion depletion zone at the anodic side of a cation-selective membrane became the unprecedentedly active research field, since the multiscale couplings of an extremely low concentration distribution [3, 5], an amplified electric field [2, 87] and an electro-convection [43, 66, 88, 89]/surface-conduction [11, 22, 45] at the micro-nano interface were tightly involved. While the classical theory has considered a diffusion and a drift ionic transportation to predict a linear concentration gradient near the membrane [35], the visualization of strong vortical flow inside the ion depletion zone has proved the significant role of the electro-convections [1] and the overlimiting conductance (OLC) measurements

with a confined microchannel structure unveiled the contribution of the surface conduction to overlimiting current [45]. Therefore, the comprehensive understandings of the classical diffusion-limited theory as well as the newly investigated electro-convection and surface-conduction were demanded for the complete pictures of the ion depletion zone.

More importantly, the electrolyte concentration profile inside the ion depletion zone is one of the most essential fingerprints for ICP phenomenon together with *I-V* responses (*i.e.* Ohmic-, limiting-, and overlimiting-current), since it would not only reflect the ion transportation through the membrane but also determine several important parameters for developing engineered ICP applications. Recently a number of experimental and simulated demonstrations had reported for the basic structure of the profile [9, 38, 40, 88, 90]. While the classical diffusion limited theory had suggested a linear concentration profile (*i.e.* diffusion layer) from the membrane to the bulk, a strong convection involved to produce the profile as the combination of the extended space charge layer, the mixing layer at a near-zero concentration and the diffusion layer. From these

publications, one would expect the monotonic function of the electric field so that the associated electrokinetic slip velocity inside the ion depletion zone should be monotonic as well.

In this work, the high-resolution electrokinetic slip velocity profiles along the ion depletion zone were measured by local-trapping the vortices in micro-grooves, leading non-monotonic velocity peak that cannot be explained by the aforementioned studies. Under the assumption that the shells of cations were stripped out [91-95] with the amplified electric field inside ICP layer, the mobility of the cation steeply increased over the threshold electric field, developing a stepwise concentration distribution. In the meantime, the nontrivial peak was attributed as the differential form of such stepwise concentration changes which strongly drove the diffusioosmotic contribution to the local slip velocity inside the ion depletion zone, while the diffusioosmosis had been neglected in the system involving a strong convection (high Peclet number regime). As a tangible evidence, a direct measurement of extracted samples from the ion depletion zone using a mass spectrometry confirmed the non-negligible

contribution of the diffusioosmosis inside the ion depletion zone.

5.2 Experimental setup

A polydimethylsiloxane (PDMS) microchip incorporated with Nafion nanoporous membrane was fabricated as shown in Figure 31 (a). The main microchannel had micro-grooves along each wall (see the inset of Figure 31 (a)). The details of the fabrication steps and the geometrical information were given in supporting information. The grooves were able to trap the flow trackers (diameter of canola oil droplets = ~2 um) and they rotated only inside the grooves with an angular velocity that was proportional to the local electrokinetic slip velocity because of the low surface charge density of oil droplets. A fingerprinted *I-V* responses were measured for various microchannel heights and the overall *I-V* behaviors were identical at the height over 200 um with 20 um X 20 um square grooves, eliminating the cross-talk between each grooved wall. See supporting information for this test.

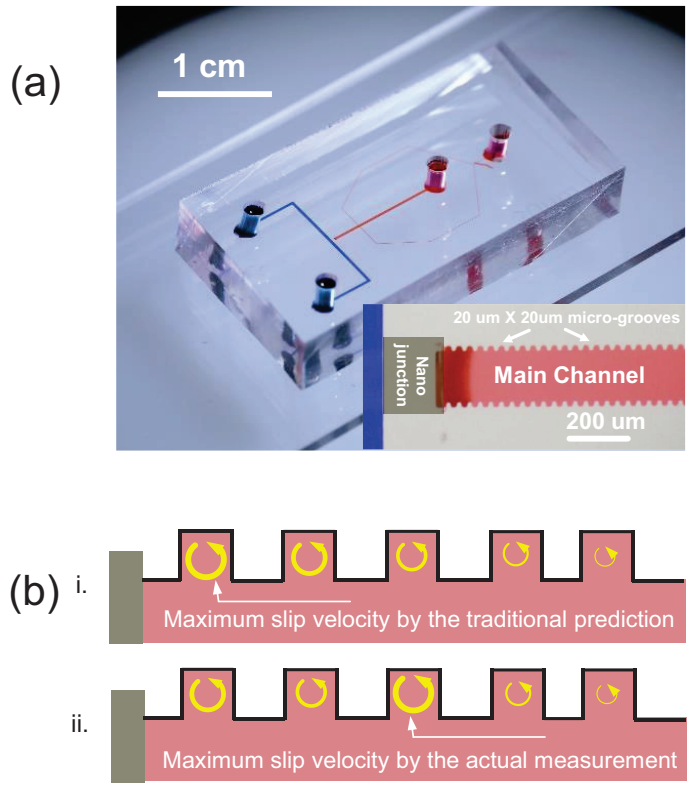

Figure 31 (a) An image of the micro/nanofluidic device that had micro-grooves along the main microchannel. Numbers in the inset pointed the numbering of each groove. (b) Schematic diagrams of the trapped vortices in the micro-grooves by i. the mean field model with constant mobility and ii. the actual measurement. The thickness of arrows indicated the magnitude of the rotational speeds.

5.3 Result and discussion

According to the mean field model with constant mobility, the magnitude of the rotational speed should monotonically decrease (the fastest near the membrane and the slowest near the boundary of ICP layer as shown in Figure 31 (b)-i), since the electric field should be a monotonic function. However, the speeds were measured with a high speed camera and the fastest slip velocity appeared in the middle of ICP layer as a schematic diagram shown in Figure 1(b)-ii. See actual experimental video in supporting information. The speeds were quantified as shown in Figure 32 (a) - (b) for LiCl and NaCl 1 mM solution, respectively. The same experiments with lower bulk concentrations (0.1 mM and 0.01 mM) for stronger ICP formation were conducted and it was found that the locations of peak were measured to be identical, since the system fell into the surface-charge-governed regime [32] (*i.e.* independent from bulk concentration) with the same length of ICP layer. See the details in supporting information. The mathematical function of curve fitting was arbitrarily chosen just for the clear visualization of the experimental plot. See the supporting information for the

fitting equations and fitting parameters. The emergence of this nontrivial velocity distribution far from the theoretical prediction has to be differently explained only with the electroosmotic flow. Note that the minimum resolution of the measurement was 20 um due to the fabrication limitation of microgrooves.

Although the mobility of ions has been usually treated as a constant quantity, the mobility can be modified by the fact that the extremely high electric field can strip the hydrated shell of the ionic species [91-95]. Due to the reduced diameter by the stripped shell, the mobility of the ion should become faster based on Stokes-Einstein relationship (mobility is inversely proportional to diameter). Thus, the hypothetical mobility change as shown in the first plot of Figure 32 (c). (The plots in Figure 32 (c) were only for the case of LiCl.) The mobility altered at a threshold electric field. According to a previous literature [96], the mobility of Li^+ of the dehydrated state was set to 6 times higher than that of the hydrated state. Typical intensity of the threshold electrical field was reported to be MV/m ~ GV/m in a gas phase [97], but the value reduced to few 0.01 MV/m ~ 0.01

GV/m in a liquid phase due to the large permittivity of liquid ($\varepsilon_{gas} \approx 1$ and $\varepsilon_{water} \approx 80$) and this magnitude was achievable in the ICP layer by the amplified electrokinetic response. Direct experimental evidences for the induced high electric field inside the ICP layer was previously reported by our group [2, 9]. In this paper, we periodically installed metal microelectrodes inside a microchannel and measured electric fields directly both inside and outside the ICP layer. This report quantitatively showed that the high electric field (~0.1 MV/m) was induced only inside the ICP layer, while the field was the same as the externally applied electric field (~3,000 V/m) outside the ICP layer. In addition, other groups also showed that electric field generated inside the ICP layer was amplified over one hundred times than outside the ICP layer using theoretical analysis as well [34, 39].

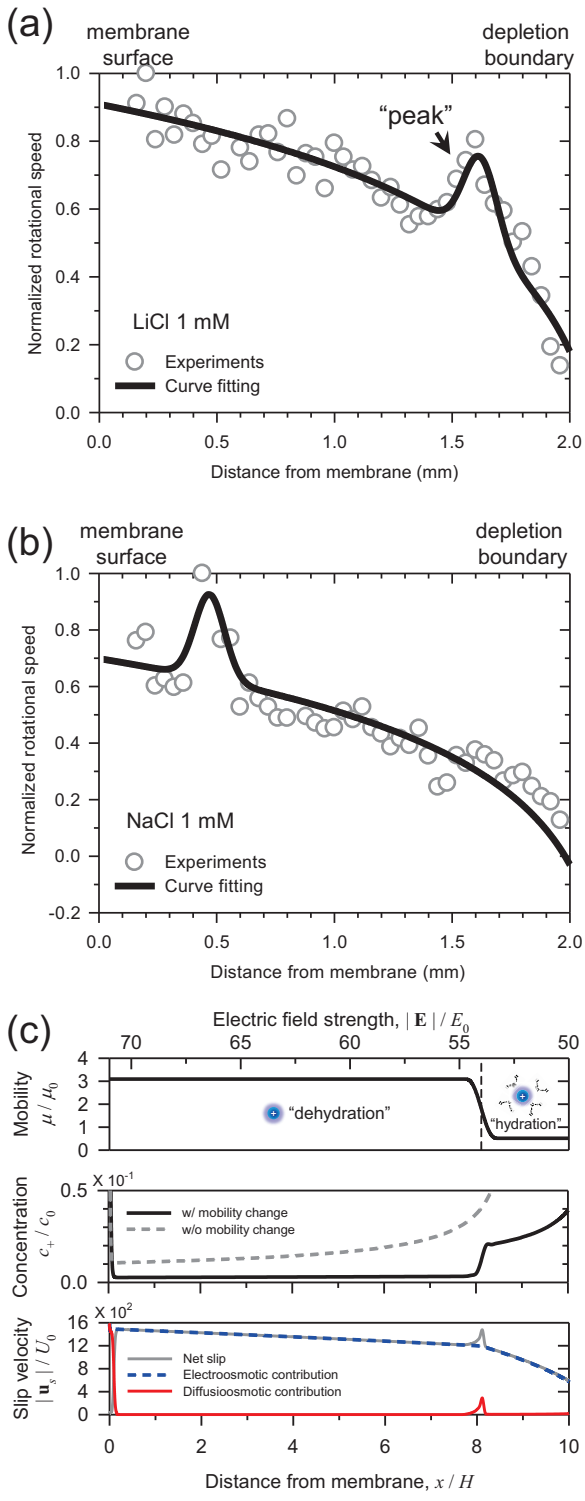
(a)
membrane surface
depletion boundary
"peak"
Normalized rotational speed
LiCl 1 mM
Experiments
Curve fitting
Distance from membrane (mm)
(b)
membrane surface
depletion boundary
Normalized rotational speed
NaCl 1 mM
Experiments
Curve fitting
Distance from membrane (mm)
(c)
Electric field strength, | E | / E0
Mobility μ / μ0
"dehydration"
"hydration"
Concentration c+ / c0
X 10-1
w/ mobility change
w/o mobility change
Slip velocity | us | / U0
X 10^2
Net slip
Electroosmotic contribution
Diffusioosmotic contribution
Distance from membrane, x / H

Figure 33. Experimentally measured rotational speeds of flow tracker inside the micro-grooves as a function of the distance inside ICP layer with (a) LiCl and (b) NaCl solution. The rotational speeds were normalized by the experimentally measured maximum speed. The curve fitting was plotted with arbitrarily chosen functions. (c) Plots for the mobility change of Li^+ as a function of an applied electric field, the concentration distribution of Li^+ and the slip velocities as a function of distance from the membrane. The mobility change and the concentration distribution were numerically obtained. The normalized parameters were as following; E_0 as the thermal voltage scale electric field (*i.e.* $RTF^{-1}L^{-1}$ where R is the gas constant, T is the absolute temperature, F is the Faraday constant, and L is the length of microchannel), μ_0 as the mobility of Cl^-, c_0 as the bulk concentration, and U_0 as the thermal voltage scale velocity (i.e. $\varepsilon\eta^{-1}L^{-1}R^2T^2F^{-2}$ where ε is the electric permittivity of water and η is the dynamic viscosity of water), respectively.

Using the field-induced mobility change of Li^+, numerically simulated cation concentration had the Heaviside distribution inside the ion depletion zone as shown in the second plot of Figure 32 (c). The threshold electric field as a modeling parameter was arbitrarily chosen to describe the location of the velocity peak inside ICP layer. This concentration distribution coincided with the previous results by measuring a local electric conductivity in which the concentration profile inside the ion depletion zone was the Heaviside function [9]. This peculiar distribution has not been predicted by any mean field model before. The concentration profile without the field-induced mobility change (gray dashed line) was a monotonically increased function shown in the second plot of Figure 32 (c).

From the fundamental electrokinetic theory [98-100], the diffusioosmosis as well as the electroosmosis is able to generate the effective slip velocity at the substrate wall in the electrochemical system. See the supporting information for the detailed equations. Since the driving force of the diffusioosmosis is the gradient of chemical potential which is defined by the logarithm of the local

concentration ($\nabla \ln(c/c_{ref}) = \nabla c/c$), one can expect the sharp driving force around the step-like change of the concentration at x / H = ~8 in the case of Li+. Consequently, the strong diffusioosmotic slip (red solid line) contributed to the net slip velocity (gray solid line) in addition to the electroosmotic slip velocity (blue dash line) as shown in the third plot of Figure 32 (c). Mathematically, $\nabla f/f$ where f is an arbitrary sigmoidal function would also have the peak shape such as the Gaussian function. Except x / H = ~8, the diffusioosmotic contribution to the slip velocity would be near-zero, since there was no significant concentration gradient in this region. Note that the steep changes around x / H = 0 were resulted from the abundant the counter-ions (c_+) adjacent to the negatively charged membrane surface due to the electrical double layer where the counter-ions were gathered to neutralize the surface charge. This counter-ion concentration at x / H = 0 was called as the Donnan equilibrium concentration (N) of which value was set to be much larger than the bulk concentration (c_0) for the case of the ideal selective membrane. One usually set the value more than $2c_0$ [101, 102]. When the ICP layer was developed near the membrane, c_+ in the

EDL asymptotically decreased from the Donnan concentration to zero-concentration [34, 39]. Since the thickness of EDL is usually 0.3 nm ~ 1 um for 1 M ~ 10^{-7} M electrolytic solution and it led considerably steep concentration gradients, the diffusioosmotic contribution (red line in Figure 32 (c)) steeply decreased (the diffusioosmosis is proportional to the concentration gradient) near $x / H = 0$.

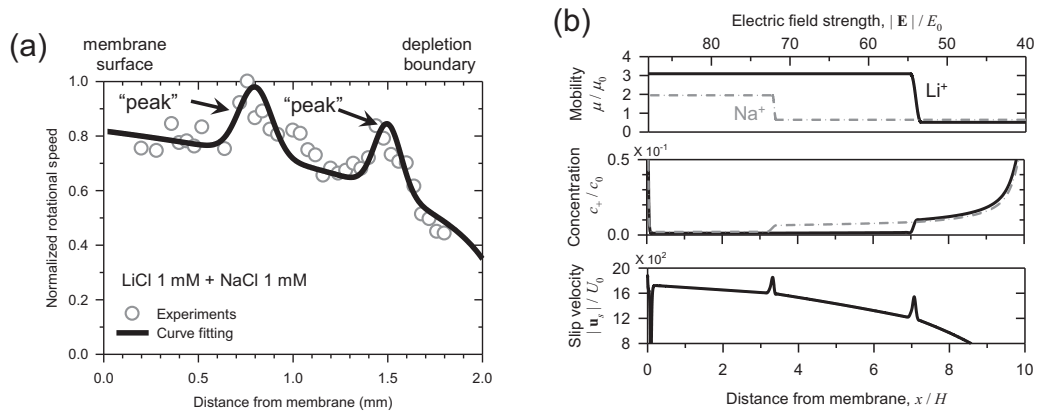

Figure 33. (a) Experimentally measured rotational speeds of flow tracker inside the micro-grooves with a multiple-cationic mixture of LiCl and NaCl solution. (b) Plots for the mobility changes of Li^+ and Na^+ as a function of an applied electric field, the concentration distribution of Li^+ and Na^+ and the slip velocities as a function of distance from the membrane. The mobility change and the concentration distribution were numerically obtained.

For a multiple-cationic mixture of LiCl and NaCl, we experimentally confirmed that the local slip velocity had two peaks as shown in Figure 33 (a). This interesting observation resulted from the hypothetical electric field-induced mobility change as well. As shown in the first plot of Figure 33 (b), each cation had the different specific threshold electric fields. The values were empirically chosen for each cation by comparing that the peak of Na^+ appeared closer to the membrane surface than one of Li^+ (see Figure 32 (a) and Figure 32 (b)). In the meantime, the mobility of Li^+ and Na^+ elevated 6 times and 4 times, respectively [96]. These combined effects led to the step-like changes of the each cation concentrations at their specific locations (x / H = ~3 and ~7 for Na^+ and Li^+, respectively in the second plot of Figure 33 (b)) and the sharp peaks of the slip velocity at the designated locations (the third plot of Figure 33 (b)). Therefore, the model considering the diffusioosmosis and the field-induced mobility change successfully illustrated the appearance of anomalous velocity peaks not only with a single cationic solution but also a multiple-cationic mixture.

The simulation results of each cationic concentration (the second plot of

Figure 33 (b)) suggested that Na^+ ion predominated in the range of $0 < x / H < 7$ and Li^+ slightly dominated over Na^+ in the range of $7 < x / H < 10$ so that there should be the inversion of the concentration values along the ICP layer. Note that the numerical model without the field-induced mobility change suggested that the concentration of Li^+ was always (slightly) higher than that of Na^+. See the SI Figure 32 (a). In order to confirm the existence of the inversion point, a 5-branched micro/nanofluidic device was fabricated as shown in Figure 34 (a). The mixture of LiCl (20 mM) and NaCl (20 mM) was pumped across the ion depletion zone and the most of ions were expelled from the zone. 20 mM of samples were used in this experiment because the concentration above 20 mM would guarantee the reliable measurement at the outlet 1 which was the closest outlet from the membrane, while the slip velocity measurement experiments were conducted with 1 mM of samples. Since the sample was continuously injected, the deionized samples were constantly collected at each branch so that the concentrations around the ICP layer was able to be discretized. See the supporting information for the experimental details. Inductively coupled plasma

optical emission spectrometry was employed to quantify the concentration of collected samples as shown in Figure 34 (b). Remarkably, the concentrations of Na^+ were higher than that of Li^+ only at the outlet 1 and 2, while the quantities were inversed at the outlet 3, 4 and 5. Most importantly, the model without the field-induced mobility change (see supporting information) would be incapable of describing the inversion of concentration inside ICP layer, since the concentration of Li^+ always higher than that of Na^+ in whole region inside ICP layer. Thus, this result would be a strong direct evidence for our model of the diffusioosmosis and the field-induced mobility change.

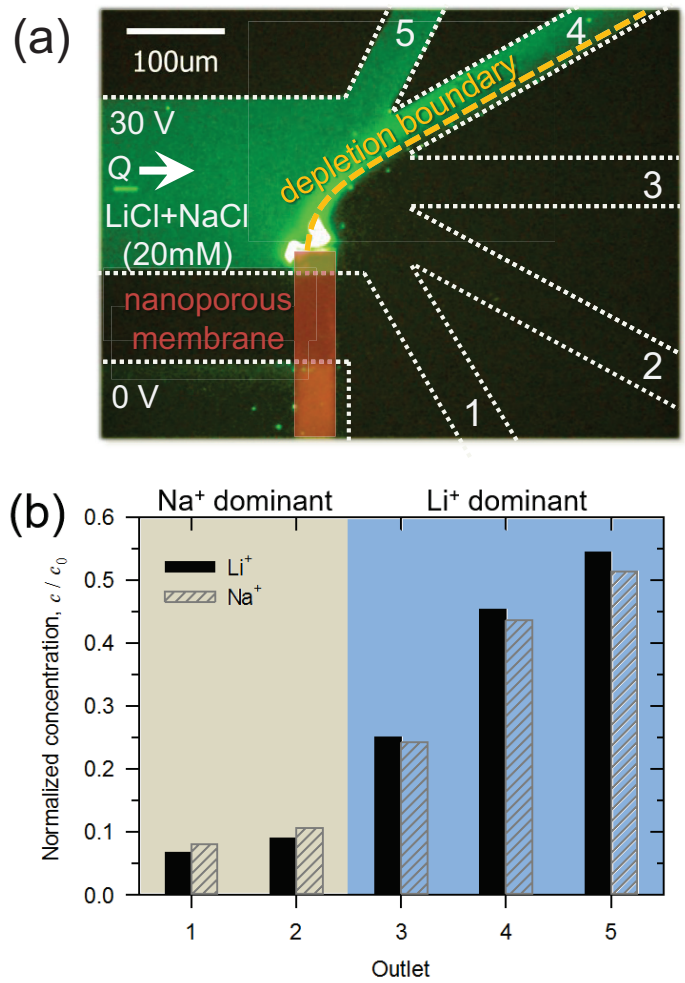

Figure 34. (a) An experimental demonstration of collecting the discretized samples from ICP layer using 5-branched micro/nanofluidic device. (b) A quantitative concentration measurement of each cation, showing the dominance was inversed between outlet 2 and 3.

The diffusioosmosis has been believed to play a significant role only for the case of zero Peclet number limit [103], *i.e*. the convection transport is negligible compared to the diffusion transport. Moreover, since ICP phenomenon had possessed a strong convective (or vortical) flow field [1, 66], one would always neglect the effect of the diffusioosmosis in ICP phenomenon. However, we demonstrated, for the first time, the *in situ* measurement of the local slip velocity inside the ICP layer as the non-monotonic function which cannot be fully elucidated by the previous insight. The formation of the slip velocity peaks within ICP layer was attributed by the contribution of the diffusioosmosis, since the local amplified electric field generated a steep concentration gradient (which is the driving force of the strong diffusioosmosis) by the hypothesis of the field-induced mobility change. This result led to the concentration profile in a form of the Heaviside function and the peak of the slip velocity inside ICP layer. Important features of these findings were validated by the direct measurement of collected samples within ICP layer.

5.4 Conclusions

Therefore, the main conclusion from this work would be that the diffusioosmosis is non-negligible even in high Peclet number limit depending on the hydrated status of major carriers. Consequently, further studies should be reserved for investigating the effect of diffusioosmosis on the ion transportation through the membrane in addition to the diffusion, the drift and the electro-convection transportation. A clear understanding of such ion transportation mechanisms inside ICP layer in micro/nanofluidic platform or porous media would be essential, not only for developing the fundamental insight of nanoscale electrokinetics, but also for guiding the engineering of ICP-based electrochemical systems, such as ion separator, fuel cells, batteries and electro-desalination systems.

Chapter 6

Overlimiting currents through ion concentration polarization layer: Hydrodynamic convection effects

This chapter consists is the basis for a paper which has been published to Nanoscale in 2014[26] and benefited from editing and directing from Prof. Sung Jae Kim. In this work, Inhee Cho conducted all the experimental setups and experimental demonstrations. Prof. Gun Yong Sung assisted the directions with a valuable scientific discussion.

6.1 Introduction

Recent advances in a nanoscale electrokinetic theory have been drawn significant attentions because new physical phenomena that have never been observed and new engineering applications based on the phenomena are actively reported. For example, electrolyte in nanostructure exhibited a semiconducting property, leading to a liquid state semiconductor such as ionic diodes and transistors[60-62, 104] and controlling ions in the electrolyte provided a

nanofluidic desalination system[3, 105] and an ion-protein preconcentration system[4, 54]. While a core mechanism of these innovative applications was a traditional electrokinetic theory, recent nanofluidic phenomena are often associated with non-traditional electrokinetic theory[28]. For example, an electroosmotic velocity near nanofluidic channel or nanoporous membrane hardly follows well-known Smoluchowski relation. Instead, the second kind of electroosmotic flow governs the electrokinetic phenomena in the nanofluidic system[1, 12, 106]. Among numerous newly-found nanofluidic phenomena, an imbalance of electrolyte concentrations nearby an electrochemical membrane under dc bias, called an ion concentration polarization (ICP), has a great potential for an engineering application since it is capable of controlling any charged species in the electrolyte on demand[4]. Due to the nanometer scales of fluidic channel, only counter-ions can pass across the nanoporous membrane, while most of co-ions are rejected to transport through the membrane[1, 66]. This property is called a perm-selectivity (or ion-selectivity) and it plays a key role to generate the ICP. Previously, while the electrical double layer overlap had

been believed to be the mechanism of the perm-selectivity, recent reports had described a relation between the bulk conductivity and surface charge of nanochannel is the key factor to initiate the perm-selectivity[6]. A cation-selective membrane submerged in electrolyte solution together with a dc bias can initiate ICP and a typical behavior is to form an ion depletion zone at the anodic side and an ion enrichment zone at the cathodic side of the membrane[65]. Since an electrolyte concentration inside the ion depletion zone became extremely low, an electrical resistance of the ICP zone significantly increased, leading to an amplified local electric field and electrokinetic vortical (or electro-convective) flows[2]. These additional transportation mechanisms observed in most electrochemical membrane systems practically initiate an overlimiting current followed after a traditional ohmic-limiting current zone that could be predicted by classical 1-dimensional diffusion-drift equations[35]. Surface conduction mechanism has been reported to be one of the key source of initiating overlimiting current especially with a thin microchannel less than 5um[11], but the dimension of microchannel (>15um) utilizing in this work falls the

dominance region of electroosmotic flow. Thus, a surface conduction effect is not considered in this study. Thus, the research about the characteristics of ohmic-limiting-overlimiting current and the way of controlling them has become a major issue of ICP theory and its applications.

Especially the limiting current is regarded as a nuisance for high energy efficient membrane systems, since it limits an upper bound of ionic current[31, 107]. In energy harvesting systems such as fuel cell or energy consuming systems such as electro-desalination system, it is definitely desirable to obtain high power level at the same power inputs, but the limiting current behavior always retards the ion transportation. Previously, numerous attempts have been carried to overcome this issue. Representing literatures are as follows. Introducing a viscous agarose gel adjacent a membrane would kill an electro-convective flow to control the current properties[108]. Both stability and current throughput were enhanced utilizing heterogeneously charged nanoporous hydrogel membrane system due to ion trading among oppositely positioned ion depletion zone and ion enrichment zone[17]. A transient effect of a strong

convective transport on the electrical properties of the microfluidic device has been reported to explain the interplay of ICP and electroosmotic flow, though the flow was in the direction normal to the membrane-electrolyte interface[90]. The restriction of the electro-convective flow by thinning microchambers that connected a nanoslot also would effectively adjust the current behavior as well[11, 67]. Similarly, an array of micro-pillar installed near the membrane can successfully control the electro-convection so that the limiting current behavior could be completely eliminated[18]. However, most of previous attempts have utilized a permanent structure so that it is impossible to tune the ohmic-limiting-overlimiting current characteristics on demands.

In this study, we experimentally demonstrated the effect of an external hydrodynamic convective flow on the ohmic-limiting-overlimiting current behavior in micro/nanofluidic modeled system. Introducing hydrodynamic convections near the membrane would restrict the expansion of ICP zone so that one can obtain a (nearly) constant electrical resistance, often leading to the complete elimination of the limiting current. Since the power required to pump

the convective sample flow was negligible compared to the total power consumption, this mechanism would be an effective mean to enhance the performance of the electrochemical membrane system. Moreover, this externally controllable hydrodynamic flow would truly realize a tunable system for an on-demand purpose.

6.2 Experimental setup

Device fabrication

We basically fabricated the one-dimensional micro/nanofluidic device consisted of main microchannel-nanojunction-buffer microchannel connection as shown in Figure 21 (a). Side microchannels were installed at the end of main microchannel so that a designated sample flow in the direction tangential to the electrolyte-membrane interface and normal to the externally applied electric field could be introduced as shown in the magnified image of Figure 21 (b). Each channel had the dimension of 200um width, 7mm length and 15um depth for the main microchannel, 200um width, 20mm length and 15um depth for the buffer microchannel and 15um width, 40mm total length and 15um depth for the side microchannels. Polymeric material, polydimethyl siloxane, (PDMS, Sylgard 184 Silicone elastomer kit, Dow Corning) was used for a building block of the device. A pre-polymer was vigorously mixed with curing agent as 10:1 and degassed in a vacuum chamber for an hour. Then the polymer solution was poured onto the prepared master that had desired device designs and cured in an

oven for 4hours. We utilized Nafion solution (20 w.t.% resin, Sigma Aldrich) as a perm-selective nanojunction material and followed a surface patterning method to fabricate the nanojunction[109]. A PDMS piece that had a straight microchannel (10mm length, 200um width and 50um depth) was reversibly attached onto a slide glass and Nafion solution was introduced into the microchannel by applying negative pressure. After removing the PDMS piece, the glass slide was heated at 95C for 5minutes to evaporate a solvent of Nafion solution. Then a solid Nafion resin was remained on the glass and it was cut with a razor blade in the middle to obtain a flat edge of the nanojunction. The main PDMS piece and the glass slide that had the Nafion nanojunction were precisely aligned using an inverted microscope (IX51, Olympus, Japan) and bonded using a plasma bonder (Cute-MP, Femto Science, Korea). Detailed schematics of each step were shown in supporting information.

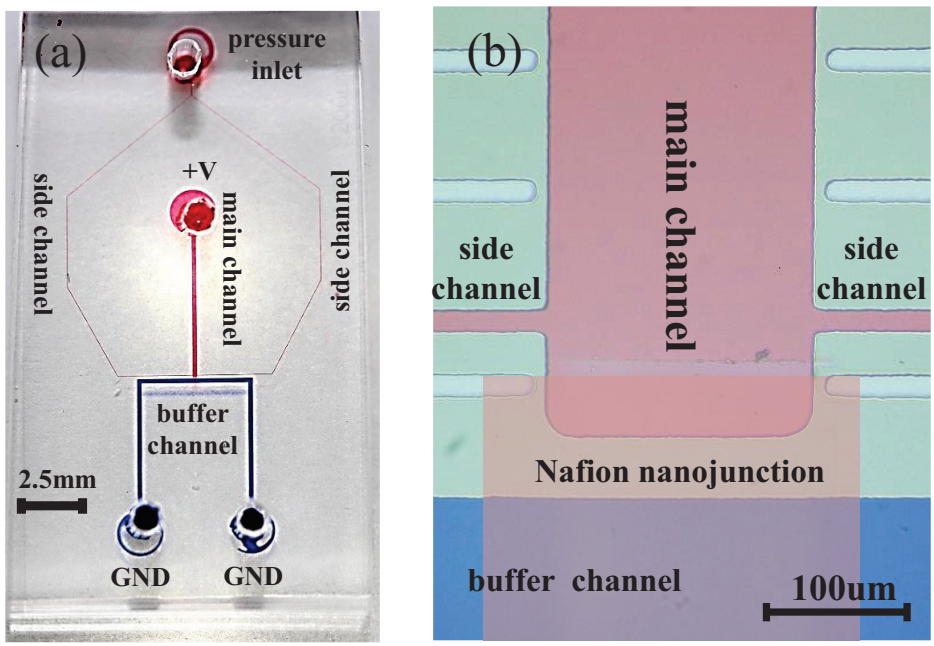

Figure 21 (a) Snapshot of the fabricated micro/nanofluidic device and (b) the magnified view near the nanojunction. Nafion polymeric nanojunction was employed to connect the main microchannel and the buffer microchannel. They were electrically connected, while only pressure fields were applied from the side microchannels for introducing a hydrodynamic convective flow adjacent the membrane.

Chemicals

We used 1mM of KCl buffer solution, since the diffusivity of K^+ and Cl^- is similar in an aqueous solution. In order to track the flow field and the ion concentration distribution, fluorescent dye (FITC, Sigma Aldrich, USA) and negatively charged micro-particles (d=1um or 0.2um, Invitrogen, USA) were mixed in the buffer solution. Prior to an experiment, the device was pre-rinsed with the buffer solution for an hour to stabilize surface properties.

Experimental setup

An external voltage was applied to the main microchannel using a source measure unit (SMU238, Keithley, USA), while the both reservoirs of the buffer microchannel were electrically grounded. A step voltage of 0.2 V ramped per 10 seconds from 0V to 15V by a customized LabView program for I-V measurement. The same procedures were repeated at least 5times for each device on more than 5 devices, guaranteeing the repeatability and reliability. The side microchannels were electrically floated, but the same buffer solution was

pumped into the side microchannels using a syringe pump (PHD2000, Harvard apparatus, USA) at various flow rates. The electrokinetic flow patterns and the concentration profiles were imaged with an inverted fluorescence microscope (IX-51, Olympus, Japan) and a CCD camera (DP73, Olympus, Japan). A commercial software (CellSense, Olympus), was used for synchronizing between the CCD camera and the microscope and analyzing the images. Detailed experimental setups were shown in supporting information.

6.3 Result and discussion

Electrokinetic flow tracking near ICP layer

As previously reported, a micro/nanofluidic system incorporated with Nafion membrane would possess an ICP phenomenon near a nanoporous membrane[4, 55, 109]. Reported properties of ICP layer are (1) significantly lower electrolyte concentrations inside the layer than one outside the layer[3], (2) amplified electrokinetic flows and electric fields due to the low concentration[2] and (3) ever-expanding length of ICP layer[9]. The presenting system also had these properties as shown in Figure 22 (a). Due to a fluidic resistance difference between the main microchannel and the side microchannels, ICP layer in presenting system were expanding upward without inflow Q from the side channels. The effect of the inflows on the system was imaged in Figure 22 (b). The flow rate was adjusted by a syringe pump connected in a pressure inlet and the exposure time of snapshot was adjusted exceptionally longer to show the flow streamline. Without the ICP formation (*i.e.* no electrical voltage), the streamline was symmetric and should flow upwardly, leading to a stagnation

point on the middle of the membrane. Therefore, the combined application of Q and V initiated the formation of a triangular shaped ICP layer in the middle of the membrane where the stagnation point was located as shown in Figure 22 (c). Interestingly, the ever-expanding property was eliminated so that the ICP layer stayed near the membrane, maintaining the triangular shape. The area of the triangle was altered by either Q or V as shown in Figure 22 (d). See the supplementary videos for detailed changes. Therefore, one can expect a constant (or slightly varied) electrical conductivity of the triangular ICP layer, while the ever-expanding ICP layer induced an dynamically decreasing electrical conductivity. Note that the values of Q (200nL/min) and V (~O(10)V) in all of Figure 22 were extraordinarily high for imaging the formation of the triangular ICP layer. The values were adjusted in moderate levels for I-V measurement experiments in the following sections.

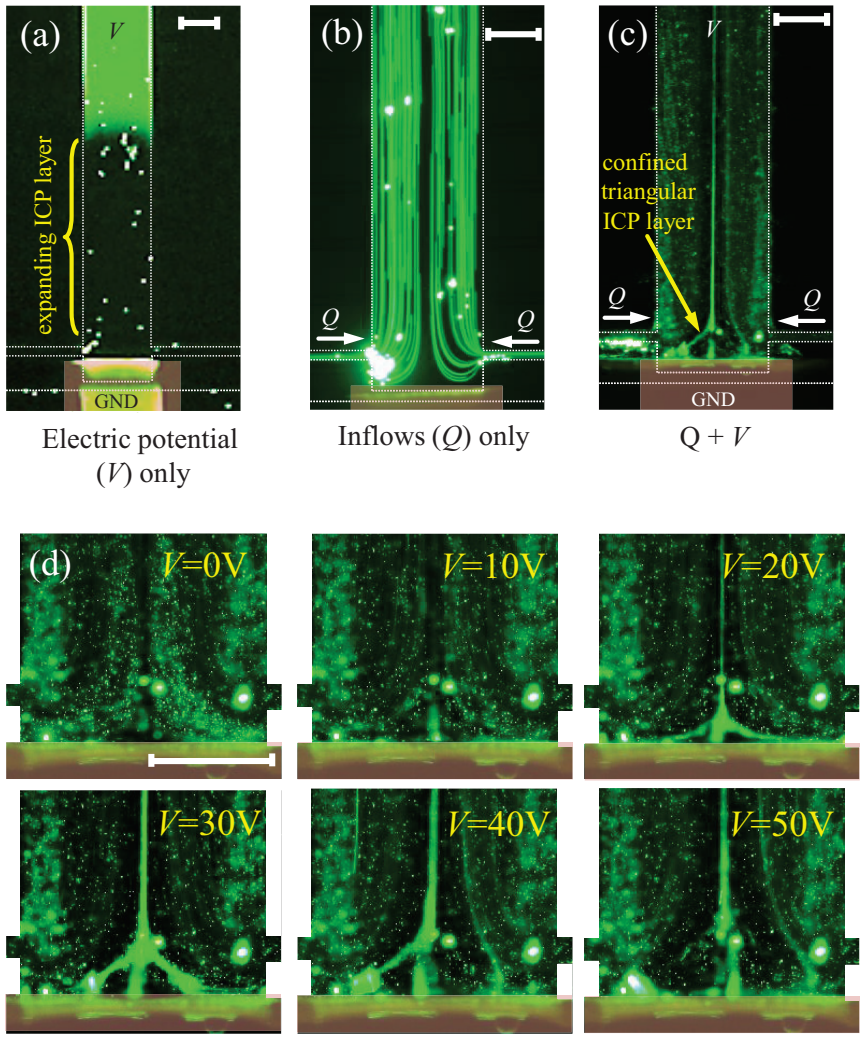

Figure 22. Microscopic fluorescent images with applying (a) an electrical potential (V) only, (b) a hydrodynamic inflows (Q) only and (c) both V and Q, showing an ever-expanding ICP layer, a stagnation point on the membrane and a confined triangular ICP layer near the membrane, respectively. (d) The

formation of triangular ICP layer with Q of 200nL/min as a function of the applied voltage. We applied higher value of voltages and flow rates than practical values for clear visualization of triangular ICP layer. See supplementary videos. All scale bars in Figure 2 were 100um.

Current-voltage measurements through ICP layer

The conductivity of ICP layer governs the total conductivity of the presenting micro/nanofluidic system, since the ion concentration inside ICP layer is extremely lower than bulk electrolyte in typical microchannels. Thus, a traditional ever-expanding ICP zone (Figure 23 (a)) resulted in a conventional ohmic-limiting-overlimiting current behavior as plotted with black triangles in Figure 23 (c). However, the application of Q from the side microchannels let the ICP layer stay near the membrane, leading a significant variation of I-V characteristics. First of all, the voltage at which the limiting current initiated increased as a function of Q. Compare the plot of black triangles to red circles in Figure 23 (c). This was because the inflows would replenish ion carriers into the

ICP layer more than the case without Q. Secondly, the limiting current region gradually disappeared as Q increased and finally eliminated at Q=40nL/min as plotted with green diamonds in Figure 23 (c). Corresponding electrokinetic flow fields were imaged in Figure 23 (b). It still showed a small triangular ICP layer and this caused a slightly deflected I-V curve. However, one can obtain the highest current values than any other cases.

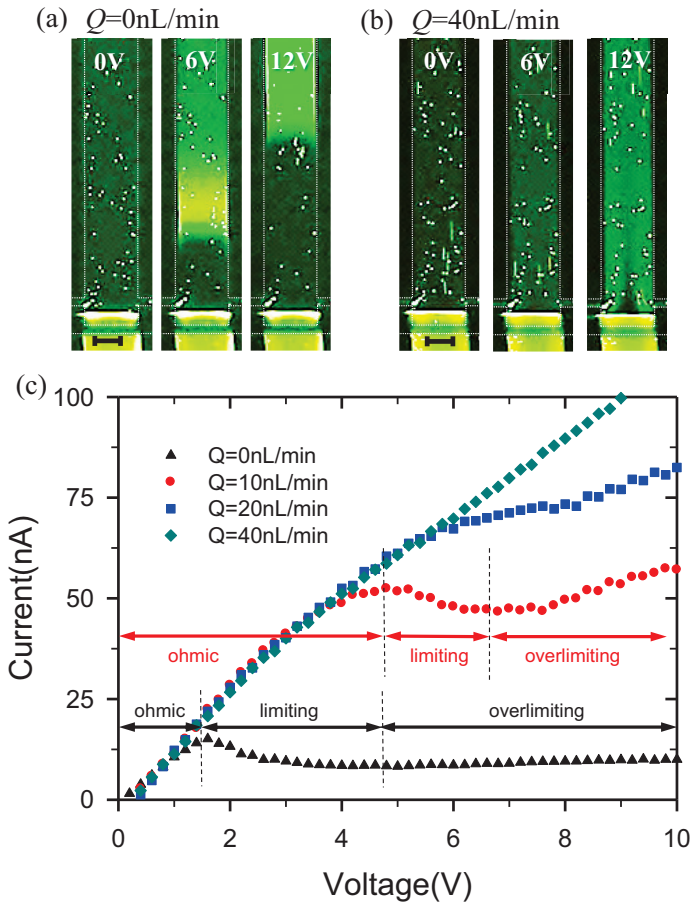

Figure 23. Microscopic fluorescent images of (a) a propagating ICP layer at Q=0 and (b) a confined triangular shaped ICP layer at Q=40nL/min as a function of applied voltages. All scale bars were 100um. (c) I-V plot as functions of V and Q. The three distinct sections, ohmic-limiting-overlimiting current regions were clearly shown in low inflow rates, while the limiting current behavior disappeared at high inflow rates.

These results in terms of conductance were plotted in Figure 24 (a). The conductance at Q=40nL/min nearly maintained its initial Ohmic conductance, while others dynamically changed as a function of applied voltages. A quantitative analysis was conducted in the sense that the thickness of diffuse layer, δ is inversely proportional to the limiting current value, *i.e.* $i_{lim}=2FDc_0/\delta$, where F the Faraday constant, D the diffusivity and c_0 the bulk concentration. Since δ is approximately proportional to the square root of the area of triangular ICP layer, overlimiting conductance and limiting current values had a close relationship with the triangular area as summarized in Figure 24 (b). The normalized values of $\widetilde{\sigma}_{over}$ and $\widetilde{i}_{lim}$ were well-matched with the inverse-root of the corresponding area. All values in Figure 24 (b) were normalized with each quantities of Q=10nL/min (i_{lim}=47.2nA, σ_{over}=3.82nS and area=24050.6um^2). The area at Q=0 and a limiting current value at Q=40nL/min was not measureable. Thus, we can conclude that all electrical quantities in this system can be precisely controlled by the confined ICP layer which was the result of hydrodynamic convective inflows.

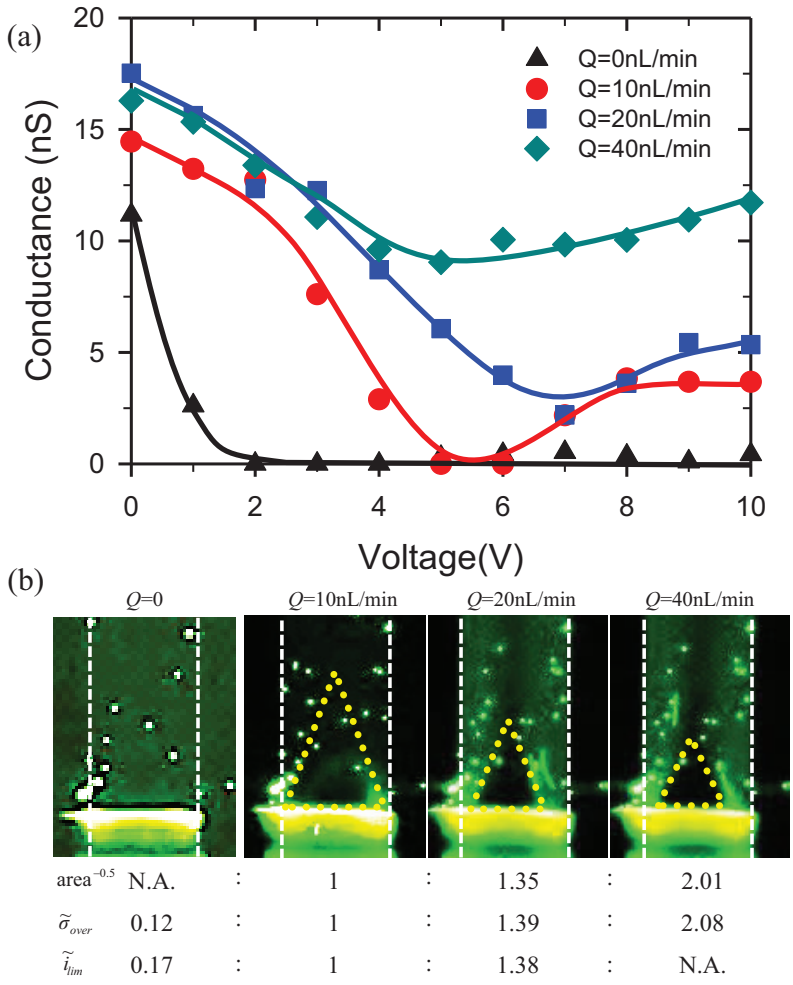

Figure 24**.** (a) A plot of system conductance as a function of inflow rates. The conductance without inflows significantly decreased, while the conductance kept its values with higher inflow rate. (b) Correlation ratios among the areas of ICP layer, overlimiting conductance and limiting current values. Tilde notations indicated a normalized value with a quantity at Q=10nL/min.

Enhancing power consumptions

All of new physical phenomena described in this work is due to introducing inflows and the Peclet number (=LU/D, where L and U is a characteristic length, velocity scale, respectively and D is the mass diffusion coefficient), which represents a ratio of convective transport rate to diffusive transport rate, can characterize the phenomena. Due to the higher velocity of inflows compared to the case of Q=0, a fluidic regime determined by large Peclet number should undoubtedly be a convection governed regime. The remaining question is how large power was consumed by the inflow pumping and how the inflow effects to the total power consumption.

To analyze a power consumption of the system, the power requirement for a hydrodynamic inflow pumping should be considered. With a constant value of Q (the dimension of device was 200um × 15um × 7mm (main channel) and 15um × 15um × 40mm (side channels)), the power requiring for the pumping through the microchannels can be calculated by pressure drops times flow rate, $W_{pump}=(\Delta p_{main}+\Delta p_{side})\times Q$. The pressure drop across the entire microchannel can

be calculated by Hagen-Poiseuille (H-P) equation, $\Delta p=12\mu QL/(wd^3)$ where μ the viscosity of sample liquid, L, w, and d the length, width and depth of microchannel, respectively[110]. By adapting μ=1.88cP and L_{main}=0.7cm and L_{side}=4cm, w_{main}=200um and w_{side}=15um, and $d_{main}=d_{side}$=15um, the power consumption, W_{pump} was

$$\left(\Delta p_{main}+\Delta p_{side}\right)\times Q=\left(\frac{12\mu QL_{main}}{w_{main}d_{main}^{3}}+\frac{12\mu QL_{side}}{w_{side}d_{side}^{3}}\right)\times Q.$$

Calculated W_{pump} were 4.96nW, 19.83nW and 79.33nW for Q=10nL/min, 20nL/min and 40nL/min, respectively. At the applied voltage of 10V, for example, an energy gain without Q was 10nA × 10V = 100nW. The voltage and current values were read in Figure 23 (c). At the same voltage, one can get the energy of 570.1nW, 824.8nW and 1106.9nW with Q of 10nL/min, 20nL/min and 40nL/min, respectively as read from Figure 23 (c). Even with the consideration of the pumping power, the energy efficiency would be significantly enhanced at 565% ((570.1nW-4.96nW)/100nW), 805% ((824.8nW-19.83nW)/100nW) and 1027% ((1106.9nW-79.33nW)/100nW) for Q of 10nL/min, 20nL/min and

40nL/min, respectively. However, unnecessary pumping power overkilled the power enhancement at lower voltage and there should be an optimum point where a pumping power and an energy gain were leveraged. In order to reflect this logic, I-V data shown in Figure 23 (c) was converted into the power enhancement (%) as a function of applied voltages as plotted in Figure 25. As we expected, the enhancement was likely to be an inverse parabolic curve so that maximum enhancement was occurred near 5V where the overlimiting current started. In case of 40nL/min, it monotonically increased to show the elimination of any limiting current behavior. The baseline at 100% was plotted with the case of Q=0. Therefore, any electrokinetic operations through an electrochemical membrane would have the best power efficiency with the voltage at which the overlimiting current was initiated. This conclusion laid in-line with the results of microfluidic electro-desalination system[111]. However, more importantly, the power efficiency would monotonically increase if the propagation of ICP layer was limited by an external hydrodynamic convective flow.

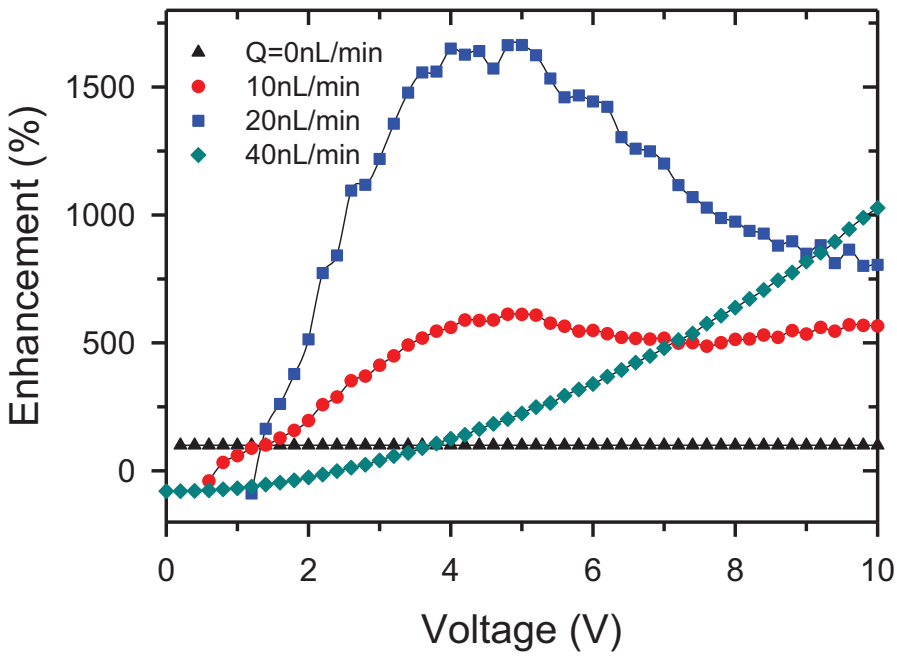

Figure 25. Plots for the enhancement of power efficiency as a function of inflow rates. It showed a maximum efficiency at lower inflow rate (*i.e.* still having limiting currents), while the efficiency monotonically increased if limiting current was eliminated by higher inflow rates.

Demonstration of nontrivial conductivity increment

Introducing additional salt via the side microchannels could increase the conductivity of the solution near the membrane, and therefore it could trivially enhance the current regardless of any other physical phenomena, leading to bypass of the limiting effect. Especially, the additional ions can directly contact with the nanojunction besides the two lower edges of the confined triangular ICP zone as shown in the schematics of Figure 26 (a). In order to eliminate this trivial increment due to the direct contact, we fabricated narrower nanojunction (width of 100um) to partially cover the main microchannel (width of 200um) as shown in Figure 26 (b). The direct contact was mostly removed by confirming the flow field and ICP layer tracking result as shown in Figure 26 (c) and *in situ* I-V responses were plotted in Figure 26 (d). The data of regular nanojunction (l_N=200um) were copied from Figure 23 (c) and they were generally identical with newly obtained plots with narrower nanojunction (l_N=100um), showing the direct contact for supplying additional ions was negligible. Instead, this confirmed that the confined area (or length) of ICP zone, which was the result of

additional convection regardless of the size of nanojunction, plays the exclusive role to determine the ionic current through nanojunction.

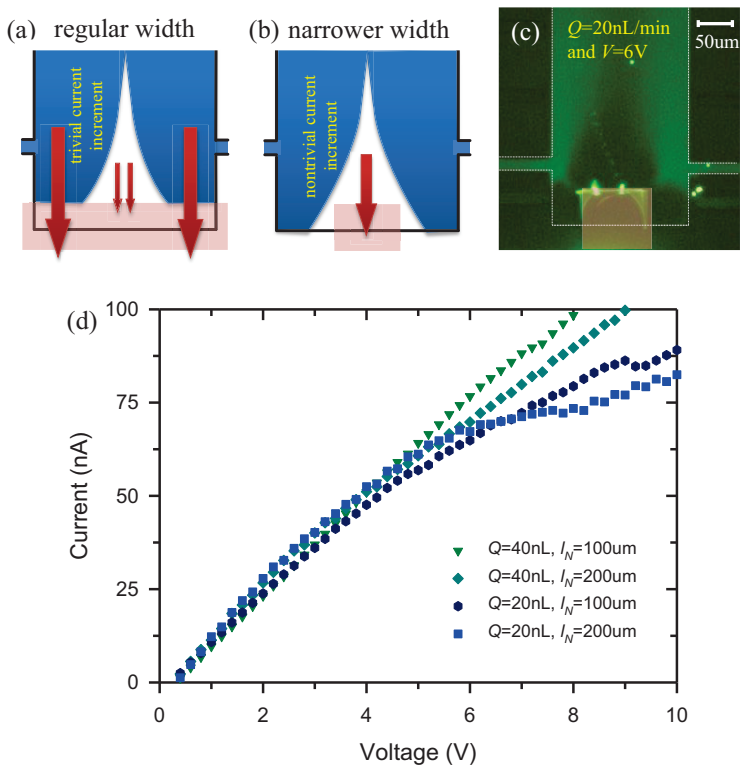

Figure 26. Schematic diagrams for (a) nanojunction with regular width and (b) nanojunction with narrower width for preventing a direct contact of additional salt inflows with nanojunction. (c) a microscopic snapshot of ICP layer formation with narrower nanojunction at Q=20nL/min and V=6V. (d) *in situ* I-V measurement with regular nanojunction and narrower nanojunction.

6.4 Conclusion

In this work, we experimentally demonstrated the effect of a hydrodynamic convective flow on current-voltage relationship through ICP layer to characterize the fundamental property of ICP layer. Introducing the hydrodynamic inflows adjacent the membrane would limit the propagation of ICP layer so that the electrical properties of whole system would be significantly improved. The correlation was elucidated using microscopic visualizations and rigorous I-V measurements in a micro/nanofluidic platform. Conclusively, the confined triangular ICP layer played the major role for determining the overlimiting current conductance as well as the limiting current value of the system. Once the limiting current behavior was eliminated by high inflows, one can achieve the monotonically increased power efficiency, while there was an optimum point where the maximum power could be obtained if the limiting current behavior still existed. The maximum power efficiency can be achieved at the external voltage right before the overlimiting current starts. The presenting mechanism would help to identify which system parameter is important and to develop a

high energy efficient electrochemical membrane system such as fuel cell, electro-desalination systems and nanofluidic biomolecular preconcentration systems, etc.

Chapter 7

Conclusions

Recent investigation has revealed out that the surface charge in the porous media or in the microchannels played a deterministic role for ion transport from aqueous solution into the ion-selective membrane. This intriguing nature should be formed of the surface conduction (SC) or electro-osmotic flows (EOF) during ion concentration polarization (ICP) phenomenon. Such transport mechanisms were subject to the multiple physics, which was tightly coupled with the amplified electric field, low concentration and the electro-convection. Thus, it is crucial for demonstrating the electrokinetic responses related to the transport mechanisms in experiments.

Here, we fabricated the PDMS microfluidic devices incorporated with the Nafion (Cation-selective nanoporous membrane) for investigating the ICP systems. With the geometrical varieties of PDMS chips, we experimentally investigated the overlimiting conductance (OLC) mechanisms by visualizing the fluorescent particles and measuring the electrical responses in the first section of

thesis. From those rigorous experiments, the significant role of ion transport through the charged microchannel walls were verified for the onset of OLC, while the particle motions during the ICP were captured in the various geometries. In addition to this, we extracted the valuable parameter (ratio of the cross-sectional area of the microchannel to the perimeter) in SC regime. This theoretical and experimental approaches enabled one to develop the microfluidic diodes without the modulation of nanochannel geometries, which could result in the cost-effective electrokinetic systems.

The investigations related to the OLC mechanisms were the most valuable work in ion-selective membrane systems, but the general lack of experimental studies has hindered one to develop the further ICP studies. Here, in the second section of this thesis, we developed the groovy microchannels for localizing and visualizing the EOF inside the ion depletion zone. Interestingly, the non-negligible diffusio-osmotic contribution were observed as well as the EOF one, which has never been predicted before. Under the assumption that the shell stripping of cations due to the amplified electric field, the concentration

distribution should possessed the sudden drop in the middle, where the diffusio-osmotic flows were located therein. This unprecedented phenomenon could lead to extract the concentrated lithium ion water in the mixture of sodium ion and lithium ion.

In the last section of the thesis, we experimentally demonstrated the effect of a hydrodynamic convective flow on the current–voltage relationship through the ion depletion zone. The hydrodynamic inflows adjacent to the membrane would restrict the expansion of the ion depletion zone so that the overall current value would be significantly improved. The correlation between the dimension of the ion depletion zone and the overlimiting conductance was validated with the visualization of microscopic images and the I-V measurements. Once the limiting current behavior was eliminated by high inflows, one can achieve the increased power efficiency. The presented mechanism would help to identify which system parameter is important and to develop a high energy efficient electrochemical membrane system such as electro desalination systems and fuel cells, etc.

In conclusively, we experimentally investigated the micro- and nano-fluidic systems regarding the ICP. This rigorous experimentation on verifying the OLC mechanisms, measuring the ESC layer responses as well as the visualizing the non-negligible diffusio-osmosis roles during ICP could lead to the further electrokinetic transport studies, but also develop the possible engineering applications such as SC diodes in microfluidic ICP systems and lithium ion water extractions etc.

Appendix

Chronopotentiometric measurement in the shear-flow assisted ICP system

A.1 Introduction

Valenca and co-worker recently demonstrated the dynamics of microvortices by ICP using chronopotentiometry for investigating the OLC conductance and the local hydrodynamics.[112] They pointed out that there existed two regimes with the time, $t=t_{EC}$, where t_{EC} is the time when EC initiated. They especially focused on the EC contribution to the voltage response when $t > t_{EC}$ while the remaining response (referred to "immediate voltage drop" in numerous researches) was responsible for the possible subject such as diffuse layer, cation-selective interface and electrical double layer when $t < t_{EC}$.

Inspired by the electrodynamics in Valenca's work, we investigated the chronopotentiometric measurement in our shear-flow assisted ICP system. Due

to the different forms of the EOI from the one of the EOF for the onset of OLC, investigating the voltage response should be reserved for the advancement in further ICP physics.

A.2 Experimental setup

Figure A1 showed the schematics of a micro- and nano-fluidic device, which consists of PDMS microchannels and Nafion nanoporous membrane (Cation-selective membrane). Microchannels were fabricated on the silicon master and we poured the mixture of Polydimethyl siloxane (PDMS, Sylgard 184 silicone elastomer kit, Dow corning) onto them. After we solidified them at 95C for 4 hours, we detached the PDMS from the master and cut the PDMS into the desirable block. We utilized Nafion resin (20 wt% resin, Sigma Aldrich) for nanojunction material, patterning on a slide glass. Then, the prepared PDMS block was irreversibly adhered to designated position on the Nafion-patterned glass substrate using plasma bonder (Cute-MP, Femto Science).

In order to generate ICP, we applied the constant currents from the end of the

main microchannel (1cm length, 100um width and 15um depth) to the Nafion nanojunction in 1mM KCl aqueous solution using a source measure unit (SMU 236, Keithley). Each chronopotentiometric measurements were done for 180 seconds at both ohmic- (1nA to 11nA) and OLC- (12nA to 29nA) regime. During these measurements, the voltage responses were recorded by the customized LabView program in every 0.18 seconds.

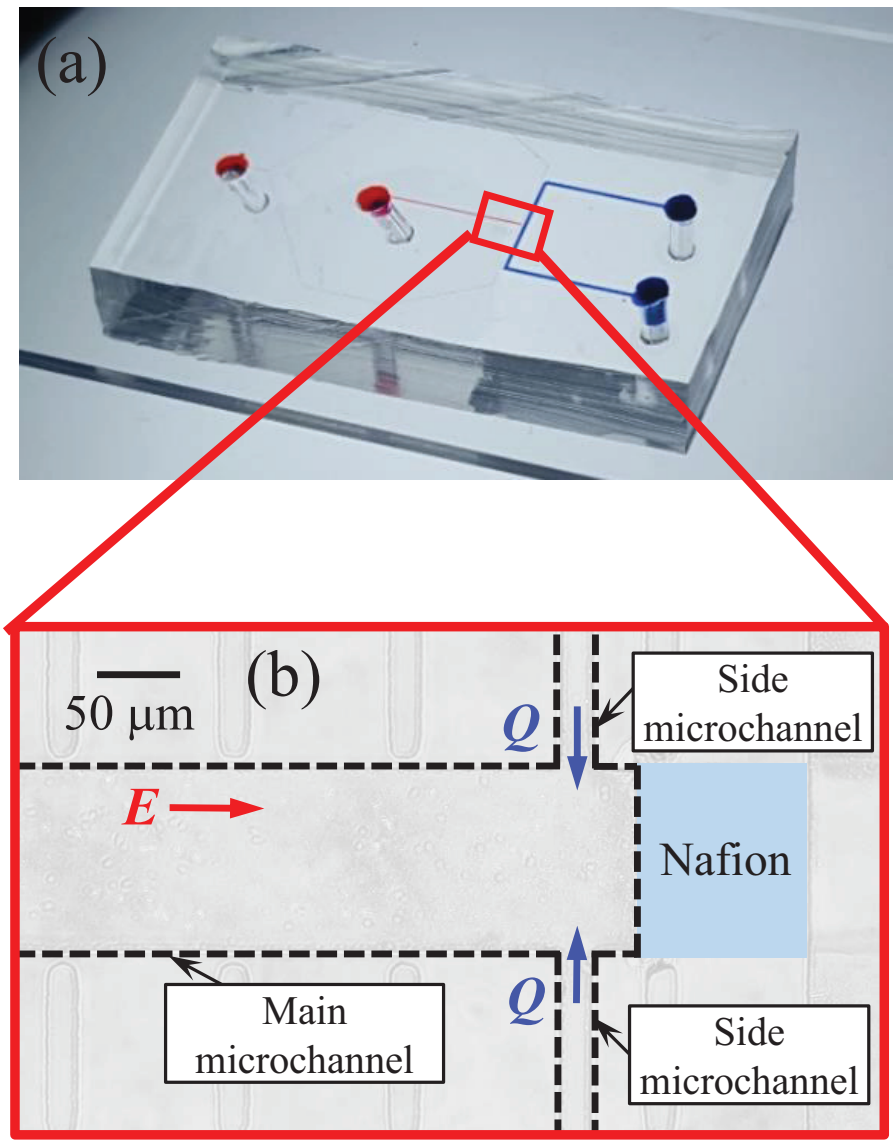

Figure A1. (a) The images of the fabricated micro-/nano-fluidic channel and (b) the magnified view of the device. Two side channel in the adjacent of main microchannel was designed in order to inject the hydrodynamic convection.

A.3 Chronopotentiometric measurement

The representative voltage-time curves at 4, 8, 14, 18 and 29(nA) shown in Figure A2 were chosen for graphical simplicity. In accordance with the previous research, we observed the two distinguished voltage responses during chronopotentiometric measurement at OLC regime, indicated by V_{1st} and V_{2nd}. Recent experiment revealed out that the micro-vortices (or electro-osmotic instabilities, EOI) was responsible for V_{2nd} during ICP. For instance, V_{2nd} was induced when the EOI was initiated ($t = t_{EC}$), and then V_{2nd} reached its maximum when the micro-vortices saturated at both the size and the speed ($t >> t_{EC}$). In case of our experiment where the OLC mechanism was lying in the EOF regime (different from the EOI regime)[112], V_{2nd} was attributed to the vortex structure by EOF under the shear flows. Thus, we confirmed the EOF contribution to the V_{2nd}. We also estimated the overlimiting conductance ($\sigma_{EOF} = I / V$) by EOF as the constant value 10 (nS) as shown in Figure A3.

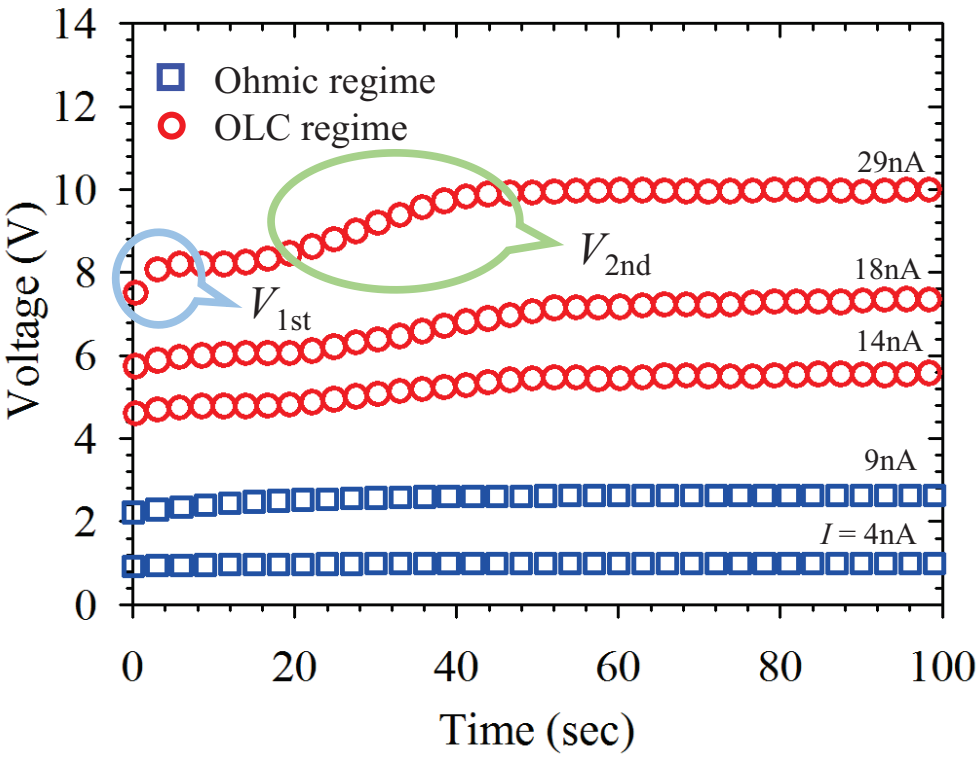

Figure A2. The experimental results of the chronopotentiometric measurement at 4, 9, 14, 18 and 29(nA), respectively. Each of the blue squares and the red circle represented the voltage responses at ohmic- and at OLC-regime, respectively. In accordance with the Valenca's work, the two voltage responses were shown during the chronopotentiometric measurement.

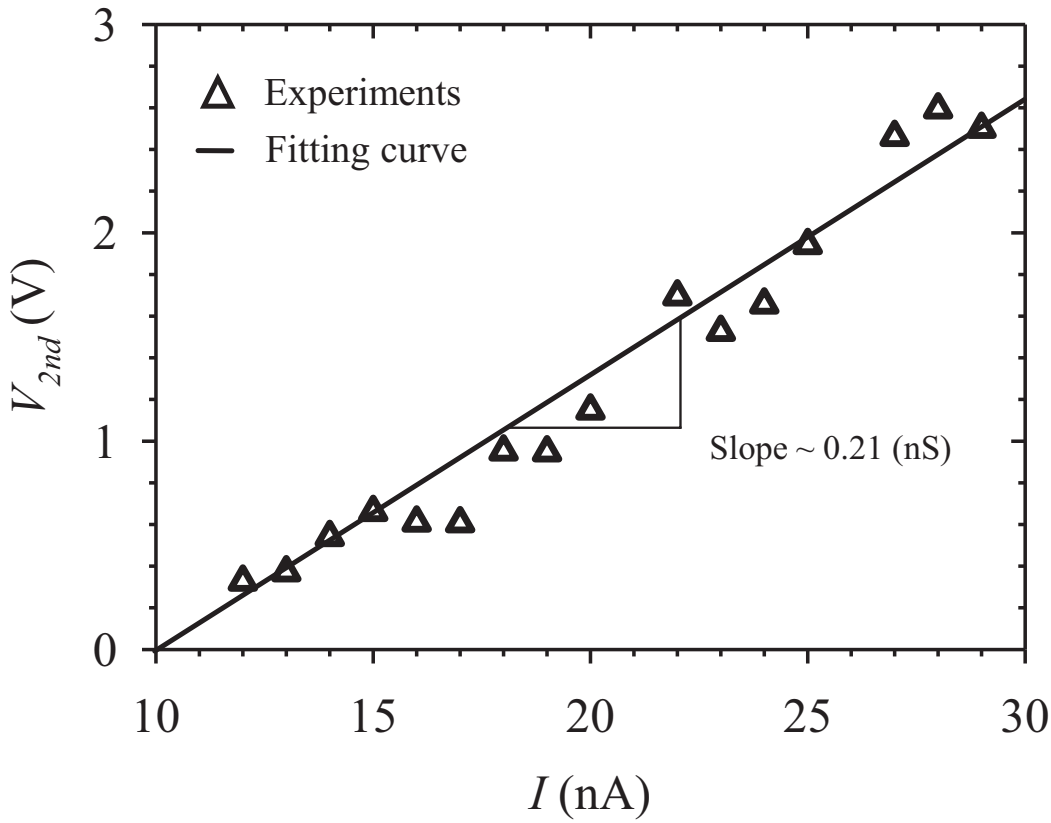

Figure A3. The overlimiting conductance (OLC) of the shear-flow assisted ICP device by chronopotentiometry. The voltage was adopted from the V_{2nd} in Figure A2. The OLC was measured to be 0.21 (nS) in our experiment.

Bibliography

[1] S. J. Kim, Y.-C. Wang, J. H. Lee, H. Jang, and J. Han, Phys. Rev. Lett. **99**, 044501 (2007).

[2] S. J. Kim, L. Li, and J. Han, Langmuir **25**, 7759 (2009).

[3] S. J. Kim, S. H. Ko, K. H. Kang, and J. Han, Nature Nanotechnology **5**, 297 (2010).

[4] S. J. Kim, Y.-A. Song, and J. Han, Chemical Society Reviews **39**, 912 (2010).

[5] G. Yossifon and H.-C. Chang, Physical Review Letters **101**, 254501 (2008).

[6] A. Mani, T. A. Zangle, and J. G. Santiago, Langmuir **25**, 3898 (2009).

[7] S. Alizadeh and A. Mani, Langmuir **33**, 6205 (2017).

[8] A. Mani and M. Z. Bazant, Phys. Rev. E **84**, 061504 (2011).

[9] S. J. Kim, S. H. Ko, R. Kwak, J. D. Posner, K. H. Kang, and J. Han, Nanoscale **4**, 7406 (2012).

[10] A. Yaroshchuk, E. Zholkovskiy, S. Pogodin, and V. Baulin, Langmuir **27**, 11710 (2011).

[11] E. V. Dydek, B. Zaltzman, I. Rubinstein, D. S. Deng, A. Mani, and M. Z. Bazant, Phys. Rev. Lett. **107**, 118301 (2011).

[12] T. A. Zangle, A. Mani, and J. G. Santiago, Chem. Soc. Rev. **39**, 1014 (2010).

[13] D. Deng, E. V. Dydek, J.-H. Han, S. Schlumpberger, A. Mani, B. Zaltzman, and M. Z. Bazant, Langmuir **29**, 16167 (2013).

[14] J.-H. Han, E. Khoo, P. Bai, and M. Z. Bazant, **arXiv:1408.4202** (2014).

[15] H. C. Chang, G. Yossifon, and E. A. Demekhin, in *Annual Review of Fluid Mechanics, Vol 44*, edited by S. H. Davis, and P. Moin (Annual Reviews, Palo Alto, 2012), pp. 401.

[16] G. Yossifon and H. C. Chang, Physical Review E **81**, 066317, 066317 (2010).

[17] P. Kim, S. J. Kim, K.-Y. Suh, and J. Han, Nano Letters **10**, 16 (2010).

[18] S. H. Ko, S. J. Kim, K. H. Kang, and J. Han, in *mTAS 2009*Jeju, Korea, 2009).

[19] R. Kwak, V. S. Pham, K. M. Lim, and J. Y. Han, Physical Review Letters **110**, 114501 114501 (2013).
[20] I. Rubinstein and L. Shtilman, Journal of the Chemical Society, Faraday Transactions 2: Molecular and Chemical Physics **75**, 231 (1979).
[21] K. T. Chu and M. Z. Bazant, SIAM Journal on Applied Mathematics **65**, 1485 (2005).
[22] C. P. Nielsen and H. Bruus, **arXiv:1408.4610** (2014).
[23] S. Hanasoge and F. J. Diez, Lab on a Chip **15**, 3549 (2015).
[24] I. Cho, W. Kim, J. Kim, H.-Y. Kim, H. Lee, and S. J. Kim, Physical review letters **116**, 254501 (2016).
[25] G. Yossifon, P. Mushenheim, Y. C. Chang, and H. C. Chang, Physical Review E **81**, 046301 (2010).
[26] I. Cho, G. Y. Sung, and S. J. Kim, Nanoscale **6**, 4620 (2014).
[27] H. Helmholtz, Annalen der Physik **165**, 211 (1853).
[28] R. F. Probstein, *Physicochemical Hydrodynamics : An Introduction* (Wiley-Interscience, 1994).
[29] R. B. Schoch, J. Han, and P. Renaud, Reviews of Modern Physics **80**, 839 (2008).
[30] K. N. Knust, D. Hlushkou, R. K. Anand, U. Tallarek, and R. M. Crooks, Angewandte Chemie International Edition **52**, 8107 (2013).
[31] J. St-Pierre, B. Wetton, G.-S. Kim, and K. Promislow, Journal of the Electrochemical Society **154**, B186 (2007).
[32] D. Stein, M. Kruithof, and C. Dekker, Phys. Rev. Lett. **93**, 035901 (2004).
[33] S. Levine, J. R. Marriott, and K. Robinson, Journal of the Chemical Society, Faraday Transactions 2: Molecular and Chemical Physics **71**, 1 (1975).
[34] M. A. K. Urtenov, E. V. Kirillova, N. M. Seidova, and V. V. Nikonenko, The Journal of Physical Chemistry B **111**, 14208 (2007).
[35] V. G. Levich, *Physico-Chemical Hydrodynamics* (Prentice-Hall, London, 1962).
[36] W. H. Smyrl and J. Newman, Transactions of the Faraday Society **63**, 207 (1967).

[37] M. Z. Bazant, K. T. Chu, and B. J. Bayly, SIAM Journal on Applied Mathematics **65**, 1463 (2005).
[38] I. Rubinstein and B. Zaltzman, Physical Review E **81**, 061502 (2010).
[39] A. S. Khair, Physics of Fluids **23** (2011).
[40] I. Rubinstein and B. Zaltzman, Phys. Rev. E **80**, 021505 (2009).
[41] D. Yan, M. Z. Bazant, P. Biesheuvel, M. C. Pugh, and F. P. Dawson, Physical Review E **95**, 033303 (2017).
[42] I. Rubinstein and B. Zaltzman, Physical Review E **62**, 2238 (2000).
[43] B. Zaltzman and I. Rubinstein, Journal of Fluid Mechanics **579**, 173 (2007).
[44] G. M. Whitesides, Nature **442**, 368 (2006).
[45] S. Nam, I. Cho, J. Heo, G. Lim, M. Z. Bazant, D. J. Moon, G. Y. Sung, and S. J. Kim, Phys. Rev. Lett. **114**, 114501 (2015).
[46] J. Schiffbauer, U. Liel, N. Leibowitz, S. Park, and G. Yossifon, Physical Review E **92**, 013001 (2015).
[47] M. B. Andersen, K. M. Wang, J. Schiffbauer, and A. Mani, ELECTROPHORESIS **38**, 702 (2017).
[48] E. Karatay, M. B. Andersen, M. Wessling, and A. Mani, Physical Review Letters **116**, 194501 (2016).
[49] M. B. Andersen, M. van Soestbergen, A. Mani, H. Bruus, P. M. Biesheuvel, and M. Z. Bazant, Physical Review Letters **109**, 108301 (2012).
[50] J. J. Krol, M. Wessling, and H. Strathmann, Journal of Membrane Science **162**, 145 (1999).
[51] A. Yaroshchuk, Advances in Colloid and Interface Science **183-184**, 68 (2012).
[52] D. Deng, W. Aouad, W. A. Braff, S. Schlumpberger, M. E. Suss, and M. Z. Bazant, Desalination **357**, 77 (2015).
[53] E. Choi, C. Wang, G. T. Chang, and J. Park, Nano letters **16**, 2189 (2016).
[54] Y.-C. Wang, A. L. Stevens, and J. Han, Anal. Chem. **77**, 4293 (2005).
[55] S. J. Kim and J. Han, Analytical Chemistry **80**, 3507 (2008).
[56] K. Kim, W. Kim, H. Lee, and S. J. Kim, Nanoscale **9**, 3466 (2017).
[57] W. Kim, S. Park, K. Kim, and S. J. Kim, Lab on a Chip **17**, 3841 (2017).

[58] C.-H. Chen, A. Sarkar, Y.-A. Song, M. A. Miller, S. J. Kim, L. G. Griffith, D. A. Lauffenburger, and J. Han, Journal of the American Chemical Society **133**, 10368 (2011).

[59] J. Choi *et al.*, RSC Advances **5**, 66178 (2015).

[60] H. Daiguji, Chem. Soc. Rev. **39**, 901 (2010).

[61] L. J. Cheng and L. J. Guo, Chem. Soc. Rev. **39**, 923 (2010).

[62] I. Rubinstein and L. Shtilman, Journal of Chemical Society Faraday Transactions II **75**, 231 (1979).

[63] P. Mao and J. Han, Lab Chip **9**, 586 (2009).

[64] S. W. Nam, M. J. Rooks, K. B. Kim, and S. M. Rossnagel, Nano Lett. **9**, 2044 (2009).

[65] Q. Pu, J. Yun, H. Temkin, and S. Liu, Nano Lett. **4**, 1099 (2004).

[66] S. M. Rubinstein, G. Manukyan, A. Staicu, I. Rubinstein, B. Zaltzman, R. G. Lammertink, F. Mugele, and M. Wessling, Phys. Rev. Lett. **101**, 236101 (2008).

[67] G. Yossifon, P. Mushenheim, and H. C. Chang, Epl **90**, 64004 (2010).

[68] P. K. Narayanan, S. K. Thampy, N. J. Dave, D. K. Chauhan, B. S. Makwana, S. K. Adhikary, and V. K. Indusekhar, Desalination **84**, 201 (1991).

[69] S. Veerapaneni, B. Long, S. Freeman, and R. Bond, Journal AWWA **99**, 95 (2007).

[70] B. S. Reto, H. Jongyoon, and R. Philippe, Rev. Mod. Phys. **80**, 839 (2008).

[71] R. B. Bird, W. E. Stewart, and E. N. Lightfoot, *Transport phenomena* (John Wiley & Sons, 2007).

[72] I. Rubinstein and B. Zaltzman, Phys. Rev. Lett. **114**, 114502 (2015).

[73] T. Pundik, I. Rubinstein, and B. Zaltzman, Phys. Rev. E **72** (2005).

[74] J. Kim, I. Cho, H. Lee, and S. J. Kim, Scientific Reports **7**, 5091 (2017).

[75] H. Lee, J. Kim, H. Kim, H.-Y. Kim, H. Lee, and S. J. Kim, Nanoscale (2017).

[76] D. C. Duffy, J. C. McDonald, O. J. A. Schueller, and G. M. Whitesides, Anal. Chem. **70**, 4974 (1998).

[77] S. Y. Son, S. Lee, H. Lee, and S. J. Kim, BioChip Journal **10**, 251 (2016).

[78] J. Kim, H.-Y. Kim, H. Lee, and S. J. Kim, Langmuir **32**, 6478 (2016).

[79] S. Xu *et al.*, Science **344**, 70 (2014).
[80] D.-H. Kim *et al.*, Science **333**, 838 (2011).
[81] C.-C. Kim, H.-H. Lee, K. H. Oh, and J.-Y. Sun, Science **353**, 682 (2016).
[82] H. Wang, V. V. Nandigana, K. D. Jo, N. R. Aluru, and A. T. Timperman, Anal. Chem. **87**, 3598 (2015).
[83] J.-Y. Jung, P. Joshi, L. Petrossian, T. J. Thornton, and J. D. Posner, Anal. Chem. **81**, 3128 (2009).
[84] G. Yossifon, Y.-C. Chang, and H.-C. Chang, Phys. Rev. Lett. **103**, 154502 (2009).
[85] J. C. T. Eijkel and A. van den Berg, Microfluidics and Nanofluidics **1**, 249 (2005).
[86] R. Mukhopadhyay, Anal. Chem. **78**, 7379 (2006).
[87] M. K. Urtenov, A. M. Uzdenova, A. V. Kovalenko, V. V. Nikonenko, N. D. Pismenskaya, V. I. Vasil'eva, P. Sistat, and G. Pourcelly, J. Membr. Sci. **447**, 190 (2013).
[88] X. Jin, S. Joseph, E. N. Gatimu, P. W. Bohn, and N. R. Aluru, Langmuir **23**, 13209 (2007).
[89] V. S. Pham, Z. Li, K. M. Lim, J. K. White, and J. Han, Phys. Rev. E **86**, 046310 (2012).
[90] R. Dhopeshwarkar, R. M. Crooks, D. Hlushkou, and U. Tallarek, Anal. Chem. **80**, 1039 (2008).
[91] C. Y. Lee, W. Choi, J. H. Han, and M. S. Strano, Science **329**, 1320 (2010).
[92] K. Kadota, A. Shimosaka, Y. Shirakawa, and J. Hidaka, Journal of Nanoparticle Research **9**, 377 (2006).
[93] J. Dzubiella and J.-P. Hansen, The Journal of Chemical Physics **122**, 234706 (2005).
[94] X. Wu, L. Lu, Y. Zhu, Y. Zhang, W. Cao, and X. Lu, Fluid Phase Equilib. **353**, 1 (2013).
[95] W. Choi, Z. W. Ulissi, S. F. E. Shimizu, D. O. Bellisario, M. D. Ellison, and M. S. Strano, Nature Communications **4**, 2397 (2013).
[96] B. E. Conway, *Ionic hydration in chemistry and biophysics* (Elsevier

Scientific Pub. Co., 1981).
[97] P. J. Taylor, A. O. Ntukogu, S. S. Metcal, and L. B. Rogers, Separation Science **8**, 245 (1973).
[98] S. S. Dukhin, Adv. Colloid Interface Sci. **35**, 173 (1991).
[99] H. J. Keh and H. C. Ma, Langmuir **21**, 5461 (2005).
[100] J. L. Anderson, Annual review of fluid mechanics **21**, 61 (1989).
[101] C. L. Druzgalski, M. B. Andersen, and A. Mani, Physics of Fluids **25**, 110804 (2013).
[102] Y. Green and G. Yossifon, Phys. Rev. E **87**, 033005 (2013).
[103] R. A. Rica and M. Z. Bazant, Physics of Fluids **22**, 112109 (2010).
[104] B. Kim, J. Heo, H. J. Kwon, S. J. Cho, J. Han, S. J. Kim, and G. Lim, ACS Nano **7**, 740 (2013).
[105] R. Kwak, S. J. Kim, and J. Han, Anal. Chem. **83**, 7348 (2011).
[106] I. Rubinstein and B. Zaltzman, Physical Review E (Statistical, Nonlinear, and Soft Matter Physics) **72**, 011505 (2005).
[107] P. Costa and B. Bosio, J. Power Sources **185**, 1141 (2008).
[108] F. Maletzki, H.-W. Rosler, and E. Staude, J. Membr. Sci. **71**, 105 (1992).
[109] J. H. Lee, Y.-A. Song, and J. Han, Lab Chip **8**, 596 (2008).
[110] G. T. A. Kovacs, *Micromachined Transducers Sourcebook* (The McGraw-Hill Companies, New York, NY, 1998).
[111] R. Kwak, G. F. Guan, W. K. Peng, and J. Y. Han, Desalination **308**, 138 (2013).
[112] J. C. de Valença, R. M. Wagterveld, R. G. H. Lammertink, and P. A. Tsai, Physical Review E **92**, 031003 (2015).

List of Publications

International Journal

Asterisk* indicate co-authorship and underlines indicate corresponding authorship.

Total citation: 84 and h-index: 4 as of November 2017

[1] Junsuk Kim, **Inhee Cho**, Hyomin Lee and Sung Jae Kim, "Ion Concentration Polarization by Bifurcated Current Path," ***Scientific Reports***, 7, 2017, p5091 (IF=5.23, Times cited: 1)

[2] **Inhee Cho***, Wonseok Kim*, Junsuk Kim, Ho-Young Kim, Hyomin Lee and Sung Jae Kim, "Non-Negligible Diffusio-osmosis inside an Ion Concentration Polarization Layer," ***Physical Review Letters***, 116, 2016, p254501. (IF=7.77, Times cited: 8) *: These authors contributed equally.

[3] Sungmin Park*, Yeonsu Jung*, Seok Young Son, **Inhee Cho**, Youngrok Cho, Hyomin Lee, Ho-Young Kim and Sung Jae Kim, "Capillarity Ion Concentration Polarization as Spontaneous Desalting Mechanism," ***Nature***

Communications, 7, 2016, p11223. (IF=11.47, Times cited: 8) *: These authors contributed equally.

[4] Sungmin Nam*, **Inhee Cho***, Joonseong Heo, Geunbae Lim, Martin Z. Bazant, Dustin Jaesuk Moon, Gun Yong Sung and Sung Jae Kim, "Experimental Verification of Overlimiting Current by Surface Conduction and Electro-osmotic Flow in Microchannels," ***Physical Review Letters***, 114, 2015, p114501 (IF=7.73, Times cited: 42). *: These authors contributed equally.

[5] **Inhee Cho**, Gun Yong Sung and Sung Jae Kim, "Overlimiting Current through Ion Concentration Polarization Layer: Hydrodynamic Convection Effects," ***Nanoscale***, 6(9), 2014, p 4620 (IF=7.40, Times cited: 25).

International Conference

Asterisk* indicate co-authorship and underlines indicate corresponding authorship.

[1] Seoyun Sohn*, **Inhee Cho***, Soonhyun Kwon, Hyomin Lee and Sung Jae Kim, "Overlimiting Conductance (OLC) under 3-Dimensional Constriction; Surface Conduction in a Microchannel," *12th international Symposium on Electrokinetics: Electrosurface Phenomena in Advanced Materials and Soft Matter,* Dresden, Germany, September 11, 2017.

[2] **Inhee Cho**, Hyomin Lee and Sung Jae Kim, "Shear Flow Assisted Characterization of the Extended Space Charge layer," *12th international Symposium on Electrokinetics: Electrosurface Phenomena in Advanced Materials and Soft Matter,* Dresden, Germany, September 11, 2017.

[3] Seoyun Sohn*, **Inhee Cho*** and Sung Jae Kim, "Micro/nanofluidic Diode using Asymmetric Ion Concentration Polarization Layer: The Rold of Surface Conduction," *69th annual meeting of Division of Fluid Dynamics, American Physical Society,* Portland, USA, Nov. 20, 2016. **(oral presentation)** *: These authors contributed equally

[4] **Inhee Cho**, Keon Huh, Rhokyun Kwak, Hyomin Lee and Sung Jae Kim, "Equivalent Electrokinetic Circuit Model of An Ion Concentration Polarization

Layer: The Contributions of Electrical Double Layer, Extended Space Charge and Electro-Convection," *69th annual meeting of Division of Fluid Dynamics, American Physical Society*, Portland, USA, Nov. 20, 2016. (oral presentation)

[5] Junsuk Kim, Hyomin Lee, **Inhee Cho**, Ho-Young Kim and Sung Jae Kim, "The Formation of Ion Concentration Polarization Layer Induced by Bifurcated Current Path," *68th annual meeting of Division of Fluid Dynamics, American Physical Society*, Boston, USA, Nov. 22, 2015. (oral presentation)

[6] Sungmin Park*, Jeonsu Jung*, Hyomin Lee*, **Inhee Cho**, Ho-Young Kim and Sung Jae Kim, "Spontaneous Salt Purification by Capillary Based Ion Concentration Polarization," *Optofluidics*, Taipei, Taiwan, July 28, 2015. **(poster presentation)** (Awarded the Best Poster Presentation.)

[7] Hyomin Lee*, **Inhee Cho***, Wonseok Kim*, Junsuk Kim and Sung Jae Kim, "Field-Induced Mobility Change Model for Ion Concentration Polarization," *Bifurcations and Instabilities in Fluid Dynamics*, Paris, France, July. 16, 2015. (poster presentation)

[8] Sungmin Park*, Yeonsu Jung*, Hyomin Lee*, **Inhee Cho**, Ho-Young Kim and Sung Jae Kim, "Capillary Ion Concentration Polarization for Power-Free Salt Purification," *67th annual meeting of Division of Fluid Dynamics, American Physical Society*, San Francisco, USA, Nov. 24, 2014. (oral presentation) *: These authors contributed equally.

[9] **Inhee Cho***, Wonseok Kim*, Hyomin Lee*, Junsuk Kim, Gun Yong Sung and Sung Jae Kim, "Anomalous Ion Concentration Distribution Inside Ion Concentration Polarization (ICP) Layer by Electrodeless Measurement," *67th annual meeting of Division of Fluid Dynamics, American Physical Society*, San Francisco, USA, Nov. 24, 2014. (oral presentation) *: These authors contributed equally.

[10] **Inhee Cho** and Sung Jae Kim, "Overlimiting current through ion concentration polarization layer: Hydrodynamic convection effects," *66th annual meeting of Division of Fluid Dynamics, American Physical Society*, Pittsburgh, USA, Nov. 2013. (oral presentation)

[11] Sungmin Nam*, **Inhee Cho***, Martin Z. Bazant and Sung Jae Kim, "Overlimiting current through ion concentration polarization layer: Experimental verifications of the surface conduction mechanism," *66th annual meeting of Division of Fluid Dynamics, American Physical Society,* Pittsburgh, USA, Nov. 2013. (oral presentation) *: These authors contributed equally.

Awards

[1] 2014.7.18. 전국 대학(원)생 에너지대회 아이디어상, 상금: 30만원

[2] 2015.7.20. 우수논문상 – 융합분야- 장려상, 상금: 10만원

[3] 2017.1.12. 우수대학원생상, 상금: 20만원

Patents

[1] Electrochemical membrane system and methods of controlling electrokinetic phenomena, registered on 2015. 3. 13., No. 10-1504109 (applied on 2014. 02. 25, No. 10-2014-0022187), Korea.

Press Archive

[1] Scientific Reports paper entitled of "*Ion Concentration Polarization by Bifurcated Current Path*" was featured on:

SNU ECE, 연합뉴스, 파이낸셜 뉴스, VERITAS Alpha, 아프로칸 뉴스룸, 디지털 타임즈

[2] Physical Review Letters paper entitled of "*Non-Negligible Diffusio-osmosis inside an Ion Concentration Polarization Layer*" was featured on:

SNU ECE, 연합뉴스, 뉴시스, 뉴스1, 아프로칸, 동아사이언스

[3] Nature Communications paper entitled of "*Capillarity Ion Concentration Polarization as Spontaneous Desalting Mechanism*" was featured on:

SNU ECE, 포커스 뉴스, 동아사이언스, etnews

[4] Physical Review Letters paper entitled of "*Experimental Verification of Overlimiting Current by Surface Conduction and Electro-osmotic Flow in Microchannels*" was featured on: SNU ECE, 연합뉴스, 헤럴드 경제, 중도일보, 아시아경제, 동아사이언스

초 록

전해질 수용액에서부터 이온선택성 분리막까지 전기동역학적 이온전달현상의 핵심 메커니즘은 전기유동(Electro-osmotic instability, EOI)으로 분석되었다. 해당 유동장은 2000년대에 개발된 랩온어칩(Lab-on-a-chip)기반의 마이크로유체역학 시스템으로 규명되었고, 연관된 기저의 물리현상인 전기장/농도장까지 확인되었다. 하지만, 마이크로 채널의 벽면전하 효과를 고려한 전기동역학 분석에 따르면, 마이크로 채널에서는 표면 전도 (Surface conduction, SC) 혹은 전기삼투유동 (Electro-osmotic flow, EOF)이 전기유동(EOI)보다 이온전달현상에 결정적인 역할을 한다는 것이 밝혀졌다. 따라서, 해당 메커니즘에 대한 실험적 검증에 대한 필요성이 대두되고 있다. 또한 마이크로채널이 결부된 이온농도분극(Ion Concentration Polarization, ICP) 시스템에서 전기장/농도장 등을 다각도로 분석방법의 필요성 또한 요구된다.

따라서 이 논문의 첫번째 장에서는, 랩온어칩 시스템인 PDMS 마이크로 채널 구조의 단면을 효과적으로 조절함으로써, 이온농도분극 현상 중의 표면전도와 전기삼투유동의 전달현상을 실험적으로 규명하였

다. 또한, 표면전도가 지배적인 영역에서는, 채널의 둘레의 길이와 단면적의 비율이 중요한 파라미터임을 추가로 제시하였다. 이는 전해질 수용액과 맞닿은 벽면이 높아질수록 표면전하효과로 인한 이온전달수송이 극도로 증가함을 의미하며, 이후 이온정류장치 개발 등에 큰 기여할 것이라고 기대한다.

나아가 두번째 장에서는 이온공핍층 내부의 지엽적 전기유동을 가시화하여 농도장/전기장을 계산할 수 있는 장치를 고안하였다. 제작된 그루브 마이크로 채널은 이온공핍층 전체의 전기유동의 모습을 관찰할 수 있었는데, 흥미롭게도 전기유동 이외의 확삼삼투유동(Diffusio-osmotic flow) 이 추가로 있다는 점을 세계최초로 밝혀내었다. 일반적으로, 확산삼투유동은 농도장 변화가 급격하거나 매우 낮은 농도일 때 발현된다. 이온공핍층은 일반적으로 낮은 농도장을 유지하는 한편, ICP의 유동장 불안정성을 야기하는데, 이는 확산삼투유동의 영향임을 증명하였다. 나아가 양이온의 종류에 따른 확산삼투유동 현상을 미세유적 추적 방식과 질량분석기 측정 방식으로 최종 검증하였다.

마지막으로 세번째 장에서는 ICP 시스템의 전력 문제와 그를 해결하는 방법을 제시하였다. 해당 전력문제를 극복하기 위해, 기존에는 영구

적인 구조물 (기둥 어레이 또는 스페이서)를 삽입하거나 이종 멤브레인 시스템을 제안하였다. 이러한 시스템들은 공통적으로 이온공핍층의 크기를 조절한다는 데에 공통점이 있다. 이 문제에 착안하여, 우리는 이온공핍층을 외부의 유압으로 조절하는 소자를 제안하였다. 실험을 통하여 이 소자는 이온공핍층을 효과적으로 제어할 수 있음을 보였을 뿐만 아니라, 전류-전압 특성 그래프에서도 한계전류값을 없앨 수 있다는 것 또한 밝혀내었다. 나아가 이 시스템은 적은 외부 유압으로 큰 전류값을 얻어낼 수 있다는 점에서, 전기화학분리막 시스템을 이용한 시스템의 전기 효율을 크게 높일 수 있다는 장점이 있다

본 논문에서는 랩온어칩 시스템에서의 이온농도분극 현상을 유동가시화를 통해 기저의 물리현상을 관찰 및 측정했을 뿐만 아니라 이온전달현상의 벽면전화 효과를 증명하였고, 나아가 유체인가시스템을 고안하여 전기 효율을 극대화시키는 방법을 제안한다.

주요어 : 이온농도분극, 과한계전류, 유체인가시스템, 확산삼투유동

학 번 : 2012-23239